Jour. of the KGS, Vol. 24, No. 3. March 2008, pp. 35~51

# Development of Modified Disturbed State Concept Model for Liquefaction Analysis

## 액상화 해석을 위한 수정교란상태개념 모델 개발

Park, Keun-Bo[1] 박 근 보 Choi, Jae-Soon[2] 최 재 순

Park, Inn-Joon[3] 박 인 준 Kim, Ki-Poong[4] 김 기 풍

Kim, Soo-Il[5] 김 수 일

## 요 지

본 논문에서는 액상화 해석에 관한 DSC 모델을 실험 및 해석적 관점에서 그 적용성을 평가하였다. 포화 사질토의 동적거동을 보다 정확히 예측하기 위해 DSC 모델을 유효응력 경로와 과잉간극수압 발현에 기초하여 수정하였다. 액상화에 대한 동적거동 및 DSC 모델에 대한 매개변수 산정을 위해 정적배수삼축시험과 반복 비배수삼축시험을 상대밀도와 구속응력에 따라 수행하였다. 유효응력 경로와 과잉간극수압의 항으로 액상화 상태를 분류하고 수정된 DSC 모델을 적용시켜 액상화 해석을 수행하였다. 제안된 방법을 토대로 DSC 모델과 제안된 DSC 모델에 대한 액상화 해석을 상대밀도와 구속응력에 따라 비교하였다. 비교 결과 수정 모델은 액상화 시작점 및 동적거동을 보다 정밀하게 평가하였고, 입력변수의 수가 감소하고 산정방법이 간편해졌다.

## Abstract

In this paper, the application of the DSC model to the analysis of liquefaction potential is examined through experimental and analytical investigations. For more realistic description of dynamic responses of saturated sands, the DSC model was modified based on the dynamic effective stress path and excess pore pressure development. Both static and cyclic undrained triaxial tests were performed for sands with different relative densities and confining stresses. Based on test results, a classification of liquefaction phases in terms of the dynamic effective stress path and the excess pore pressure development was proposed and adopted into the modified DSC model. The proposed methods using the original and modified DSC models were compared with examples with different relative densities and confining stresses. Based on the comparisons between the predicted results using the original and modified DSC models and experimental data, the parameters required to define the model were simplified. It was also found that modified model more accurately simulate initial liquefaction and dynamic responses of soil under cyclic undrained triaxial tests.

**Keywords** : Disturbance, Disturbed state concept, Earthquakes, Excess pore pressure, Liquefaction

1 Member, Post Doc., School of Civil & Env. Eng., Yonsei Univ., uscake@yonsei.ac.kr, Corresponding Author

2 Member, Instructor, Dept. of Civil Eng., Seokyeong Univ.

3 Member, Associate Prof., Dept. of Civil Eng., Hanseo Univ.

4 Graduate Student, School of Civil & Env. Eng., Yonsei Univ.

5 Member, Prof., School of Civil & Env. Eng., Yonsei Univ.

## 1. Introduction

The excess pore pressure is an important consideration for the behavior of saturated sands under seismic loading conditions. When a dynamic force such as an earthquake is applied to saturated sands, the excess pore pressure builds up continuously with decreases of soil strength, and sands are eventually liquefied. For the assessment of liquefaction potential or susceptibility for sands, experimental investigations are often used based on cyclic triaxial tests or in-situ field tests such as SPT and CPT [Seed et al., 1983; Youd et al., 2001]. Analytical investigations based on numerical modeling and analysis have been limited to those requiring accurate description of complex undrained behaviors of saturated sands, including mobilization and accumulation of the excess pore pressure and consequent stress softening.

There have been several soil models for describing undrained behaviors of fully saturated sands under dynamic loading conditions [Finn et al., 1977; Iai et al., 1992; Desai and Ma, 1992; Desai et al., 1998]. Representative examples are those of Finn et al. [1977], Iai et al. [1992], and Desai et al. [1998], all of which are based on the effective stress concept. According to Finn et al. [1977], mobilized excess pore pressures under undrained conditions can be determined as a function of drained volumetric strains. In this approach, different stress-strain relationships are considered for initial loading and reloading stages for the calculation of excess pore pressure development and dissipation.

For the analysis of liquefaction potential, Iai et al. [1992] defined an initial liquefaction occurrence at the liquefaction front state given by the phase change line (e.g., phase transformation line). The phase change line represents a boundary between contractive and dilative behaviors observed in dynamic effective stress paths. Disturbed state concept (DSC) was first introduced by Desai [1980] to characterize work-hardening behaviors of over-consolidated soils with reference to those of normally consolidated soils. Further development was made for the description of undrained behaviors for saturated sands afterward [Desai et al., 1991; Desai and Ma, 1992; Katti and Desai, 1994; Desai and Toth, 1996; Desai et al., 1997; Desai and Rigby, 1997; Desai et al., 1998]. In the DSC model [Desai and Ma, 1992; Desai et al., 1998], dynamic responses of soils are defined as a function of the material disturbance caused by an applied force and induced deviatoric plastic strains. The material disturbance represents changes in microstructures of a material due to an applied force from the relative intact (RI) to the fully adjustment (FA) states. Observed responses of the material are then given by relative differences between RI and FA states, which are quantified through the material disturbance.

While the DSC model has been successfully verified for many geotechnical dynamic problems [Desai et al., 1998; Desai and Toth, 1996; Desai et al., 1997; Desai and Rigby, 1997; Pal and Wathugala, 1999], those have been primarily for low excess pore water pressure and small-strain conditions. For the application to liquefaction, it has been limited to the determination of the initial liquefaction occurrence, and not been fully implemented for a whole process of liquefaction analysis, including the determination of liquefaction potential.

In this paper, the application of the DSC model to the analysis of liquefaction potential is examined through experimental and analytical investigations. For more realistic description of dynamic responses of saturated sands, the DSC model is further modified based on experimental results and soil phases observed in the dynamic effective stress path. Both static and cyclic undrained triaxial tests are performed for sands with different soil and stress conditions. Based on test results, a classification of liquefaction phases in terms of the dynamic effective stress path and the excess pore pressure development is proposed and adopted into the modified DSC model.

## 2. Disturbed State Concept

### 2.1 RI and FA States

According to the disturbed state concept (DSC) proposed by Desai et al. [1998], external forces cause changes and disturbances in the microstructure system of a material. The stress-strain response of the material at a certain loading condition is then determined from a degree of

the disturbance caused by the external force. There are two reference states defined in the DSC model: relative intact (RI) and fully adjusted (FA) states. A material in the RI state upon loading modifies continuously through a process of natural self-adjustment, and a part of it approaches the FA state at randomly disturbed locations in the material. As a result, observed or average responses of the material can be determined from responses of RI and FA states in terms of the disturbance D. This is illustrated in Fig. 1. The RI state is defined with continuum soil models, such as the elastic-plastic stress-strain models, while the FA state is defined as a response of a material at the ultimate state. In the original DSC model [Desai and Ma, 1992; Desai et al., 1998], the RI state is determined by Hierarchical Single Surface (HiSS) model [Desai et al., 1991] with the isotropic hardening and associated flow rule whereas the FA state is given by the critical state model [Roscoe et al., 1958].

From stress–strain responses of RI, FA, and observed states shown in Fig. 1, the disturbance D and effective stresses in the DSC model are given by:

$$D = \frac{\sigma_{ij}^{'R} - \sigma_{ij}^{'O}}{\sigma_{ij}^{'R} - \sigma_{ij}^{'F}} \quad (1)$$

$$\sigma_{ij}^{'O} = (1-D)\sigma_{ij}^{'R} + D\sigma_{ij}^{'F} \quad (2)$$

where D = disturbance at a current observed state; and $\sigma'^{R}_{ij}$, $\sigma'^{F}_{ij}$, and $\sigma'^{O}_{ij}$ = effective stresses at RI, FA, and observed states, respectively. Differentiating Eq. (2), the incremental formulation of the observed stress is obtained as follows [Desai, 1980]:

$$d\sigma_{ij}^{'O} = (1-D)d\sigma_{ij}^{'R} + Dd\sigma_{ij}^{'F} + dD(\sigma_{ij}^{'F} - \sigma_{ij}^{'R}) \quad (3)$$

where $d\sigma'^{R}_{ij}$, $d\sigma'^{F}_{ij}$, and $d\sigma'^{O}_{ij}$ = stress increments at RI, FA, and observed states, respectively.

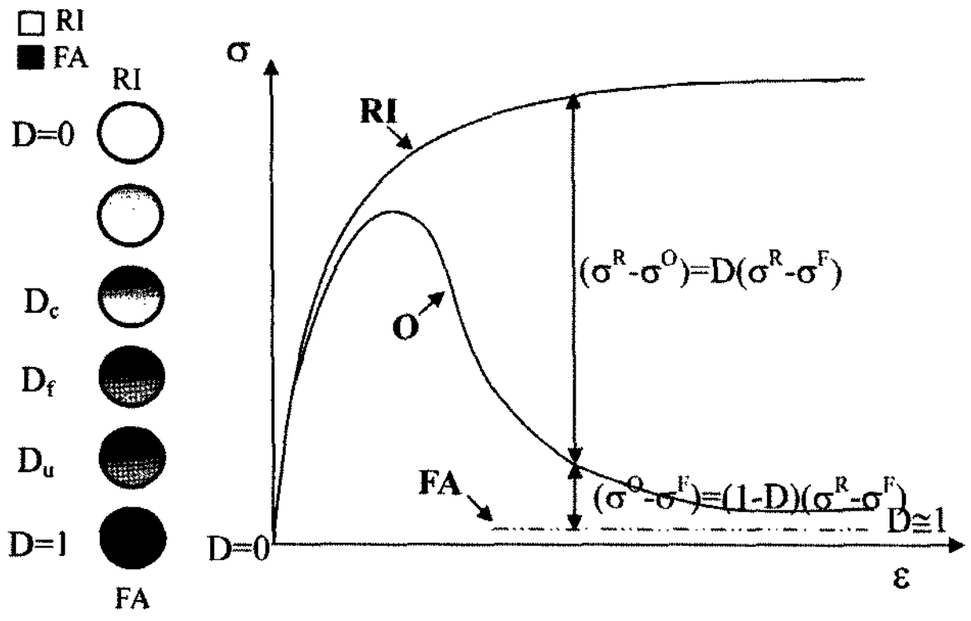

RI: Relative intact FA: Fully adjusted O: Observed

Fig. 1. Stress-strain responses with disturbed state concept (after Desai et al., 1998)

## 2.2 Disturbance

Key parameter in the DSC model is the disturbance D as it determines the stress-strain response and shear resistance at a certain loading stage. According to Desai et al. [1998], the disturbance D and deviatoric plastic strain trajectory $\xi_D$ are defined through the following relationship:

$$D = D_u[1 - \exp(-A\,\xi_D^{\,Z})] \quad (4)$$

where $D_u$, A, and Z = material constants obtained from experimental test results; and $\xi_D$ = deviatoric plastic strain trajectory. The deviatoric plastic strain trajectory $\xi_D$ in (4) is defined as:

$$\xi_D = \int \sqrt{d\varepsilon_{ij}^p d\varepsilon_{ij}^p} \quad (5)$$

where $d\varepsilon_{ij}^p$ is an increment of the deviatoric plastic strain tensor under undrained conditions. Eq. (5) represents that the deviatoric plastic strain trajectory $\xi_D$ is equal to absolute amount of deviatoric plastic strains accumulated from the initial to a given loading cycle in a dynamic loading process.

Fig. 2 shows the calculation procedure of the deviatoric plastic strain trajectory $\xi_D$ from a cyclic stress-strain response and typical disturbance curve in terms of D and $\xi_D$ for sands. As shown in the figure, values of D vary from 0 to 1 through linear increase, non-linear increase, and stabilization stages. Value of D equal to 0 represents the initial RI state while D = 1 corresponds to the FA state. From the disturbance curve in Fig. 2 (b), it is seen that there is a point of the maximum curvature (i.e., point A) before the stabilized D value equal to 1 is reached. Value of D corresponding to this point is defined as the

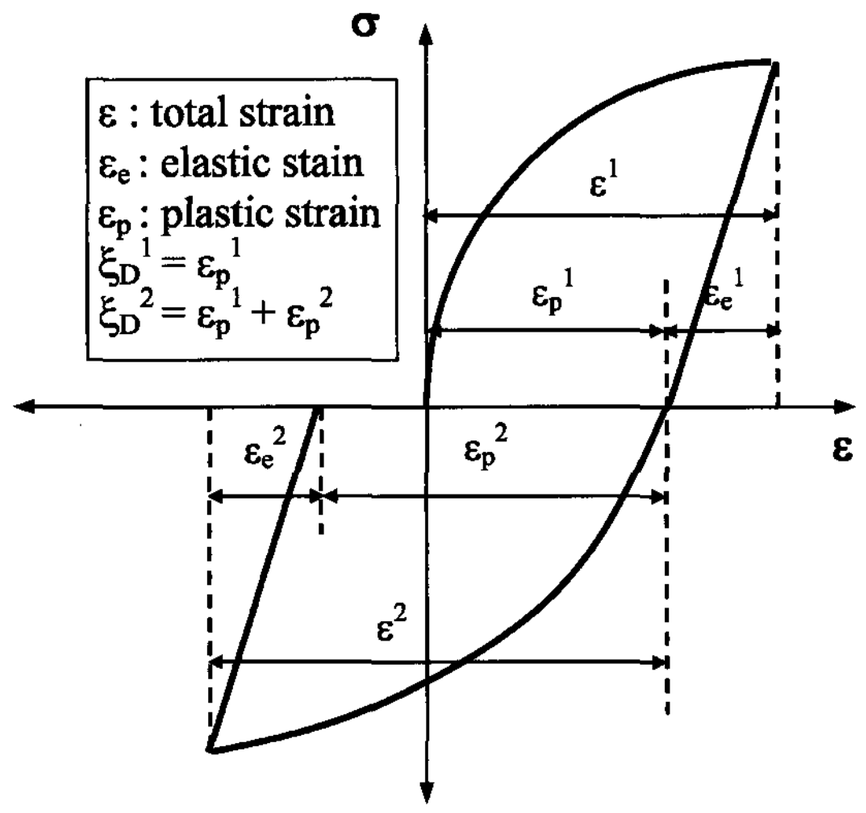


(a) determination of $\xi_D$

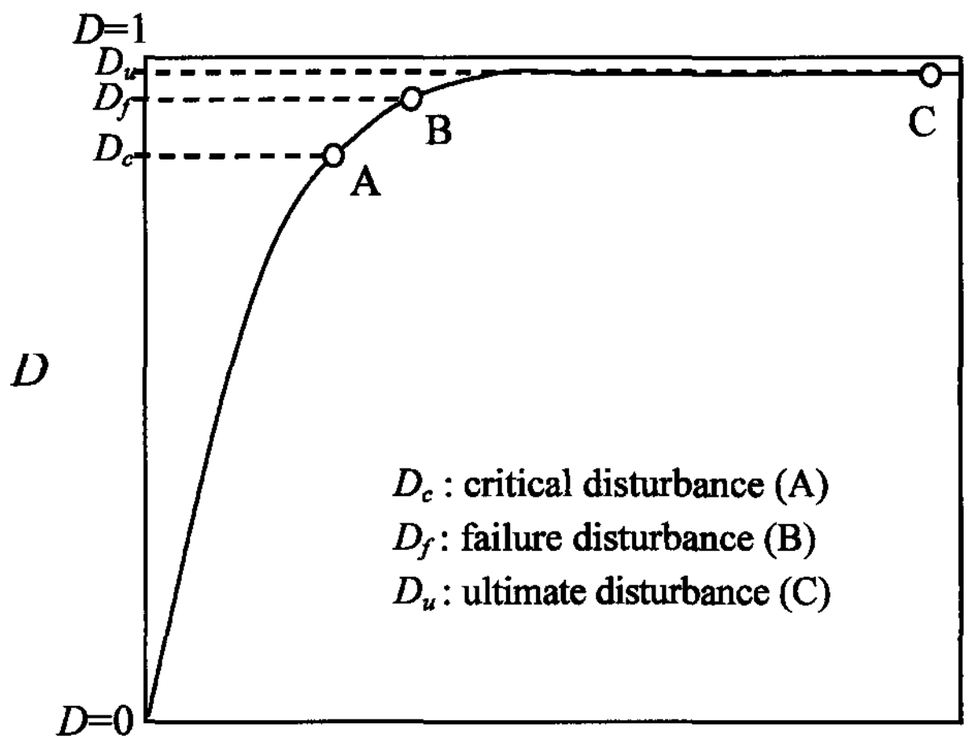


(b) disturbance function

Fig. 2. Deviatoric plastic strain trajectory $\xi_D$ and disturbance function curve (after Desai et al., 1998)

critical disturbance $D_c$. Importance and application of the critical disturbance $D_c$ to liquefaction will be discussed later.

## 2.3 Stress-Stain Models for RI and FA States in DSC

In the DSC model by Desai and Ma [1992] and Desai et al. [1998], the HiSS model [Desai et al., 1991] and the well-known critical state model [Roscoe et al., 1958] are used to define RI and FA states, respectively. The yield surface in the HiSS model for the RI state is given by:

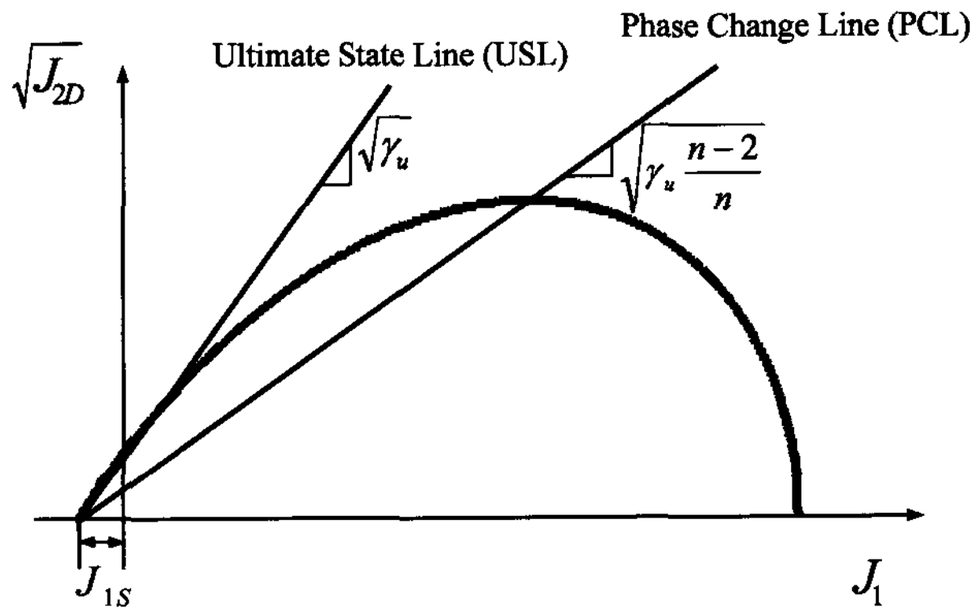


Fig. 3. Yield surface in HiSS model (after Desai et al., 1991)

$$F = \frac{J_{2D}}{p_a^2} - \left[ -\alpha \left( \frac{J_1 + J_{1s}}{p_a} \right)^n + \gamma_u \left( \frac{J_1 + J_{1s}}{p_a} \right)^2 \right] \quad (6)$$

where $J_1$ = the first invariant of the stress tensor; $J_{2D}$ = the second invariant of the deviatoric stress tensor; $J_{1s}$ = shift of $J_1$ axis for materials such as concretes which possess tensile strength; $p_a$ = atmospheric pressure in the same unit as the stress tensor; n and $\gamma_u$ = model parameters; and $\alpha$ = hardening function. The hardening function $\alpha$ can be defined in terms of the deviatoric plastic strain trajectory $\xi_D$ for undrained conditions as follows [Desai, 1980]:

$$\alpha = \frac{h_1}{\xi_D^{h_2}} \quad (7)$$

where $h_1$ and $h_2$ = hardening function parameters; and $\xi_D$ = deviatoric plastic strain trajectory defined by (5).

Fig. 3 shows the yield surface given by the HiSS model. In the HiSS model, as shown in Fig. 3, there are two reference lines defined for states of soil responses: phase change and ultimate state lines. The phase change line represents a boundary under which soils are contractive and a point where states of soil responses were changed. Once a stress path meets the phase change line, a sand becomes dilative with a stress path approaching to the ultimate state line. The ultimate state line represents a state of no volume change corresponding to the critical state line in drained conditions.

## 3. Experimental Investigation of Dynamic Soil Responses

### 3.1 Cyclic and Static Triaxial Tests

In order to investigate detailed undrained behaviors and dynamic responses of saturated sands, both cyclic and static undrained triaxial tests were performed for different soil conditions. The testing equipment was the automated triaxial testing system manufactured by Soil Engineering Equipment®, which allows application of both cyclic and static loadings. Test soil was the Jumunjin sand, a standard sand in Korea with properties given in Table 1. For static tests, two different confining stresses ($\sigma'_c$ = 100 and 150 kPa) and two different relative densities ($D_R$ = 40 and 60%) were used. Also, two test conditions, $\sigma'_c$ = 150 kPa with $D_R$ = 40% and $\sigma'_c$ = 100 kPa with $D_R$ = 60%, were used for dynamic tests.

Fig. 4 shows loading mechanisms for cyclic and static undrained triaxial tests adopted in the present study. For cyclic triaxial tests in Fig. 4 (a), the sinusoidal type of cyclic deviatoric stresses equal to 63 and 44 kPa were applied while cyclic radial stresses were applied with a magnitude equal to a half deviatoric stress at a phase angle difference of 180°. This allows the constant mean total stress of soil samples throughout the tests. In cyclic triaxial tests, the stress-strain curve for the first compression stage represents the RI state, whereas subsequent loading cycles result in increases of the material disturbance with stress softening behavior. Fig. 4 (b) shows the loading mechanism used for static undrained triaxial tests. As shown in the figure, a combined loading condition of the axial compression (AC) and the lateral extension (LE) was adopted in the tests with constant mean total stresses throughout the tests. As a result, stress-strain curves from AC-LE static triaxial tests represent the same RI state as those from cyclic triaxial tests for the first loading cycle.

In order to maintain the sample homogeneity, test samples were produced using the undercompaction technique recommended by Ladd (1978). Soil samples for tests were prepared as follows. Firstly, test samples of a weight corresponding to a target $D_R$ value (i.e., $D_R$ = 40 and 60% in this study) were placed into the triaxial sample mold wrapped with the rubber membrane. Test samples were placed and compacted in five sub-layers. After the sample preparation, $CO_2$ gas was injected into the test sample and de-aired water was introduced for the sample saturation. This process was adopted for more effective sample

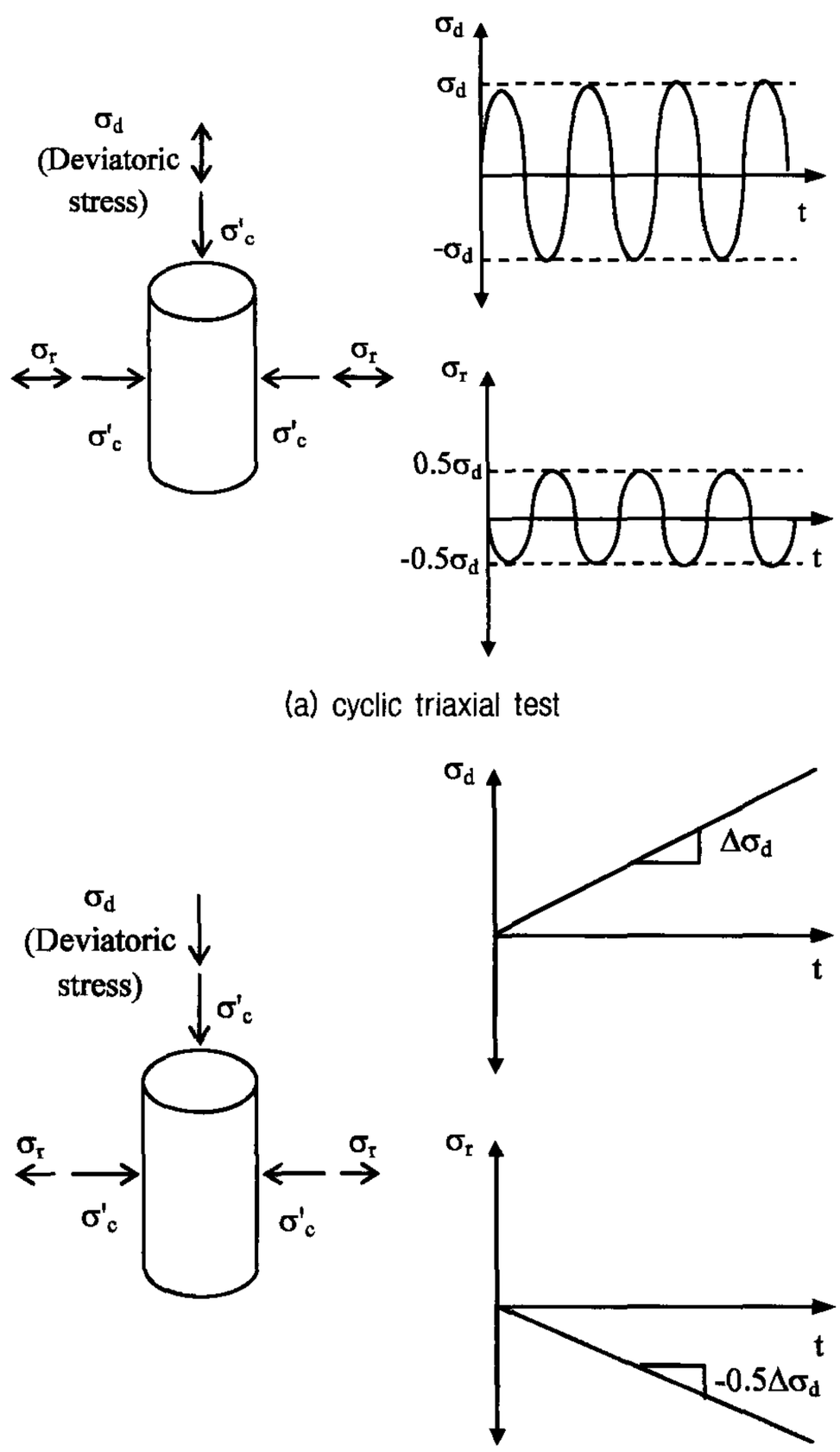


Fig. 4. Loading mechanisms

Table 1. Basic properties of Jumunjin sand

| $\gamma_{dmax}$ (kN/m$^3$) | $\gamma_{dmin}$ (kN/m$^3$) | $e_{max}$ | $e_{min}$ | GS | $D_{50}$ (mm) | $C_u$* | $C_c$** |
|---|---|---|---|---|---|---|---|
| 15.7 | 13.6 | 0.719 | 0.625 | 2.63 | 0.52 | 1.35 | 1.14 |

*$C_u$ = coefficient of uniformity, $C_c$**= coefficient of curvature.

saturation and continued for approximately 3 hours. After placing the sample into the triaxial loading chamber, a back pressure equal to 150 kPa was applied for at least 2 hours to ensure the sample saturation. Once the B value reached a value greater than 0.97, the confining stress was applied, which was maintained for approximately 1 hour. For shearing stage in static triaxial tests, a loading rate equal to 0.1% strain per minute was used, while cyclic triaxial tests were performed at a loading frequency equal to 1 Hz.

## 3.2 Test Results

Fig. 5 shows stress-strain curves, mobilization of excess pore pressures, and effective stress paths obtained from static undrained triaxial tests. As shown in Figs. 5 (a) and (b), no significant differences in stress-strain curves are observed for $\sigma'_c$ = 100 and 150 kPa. This is because the loading mechanism of AC-LE triaxial tests with decreasing radial stress compensates the effect of different initial confining stresses. Figs. 5 (c) and (d) show that

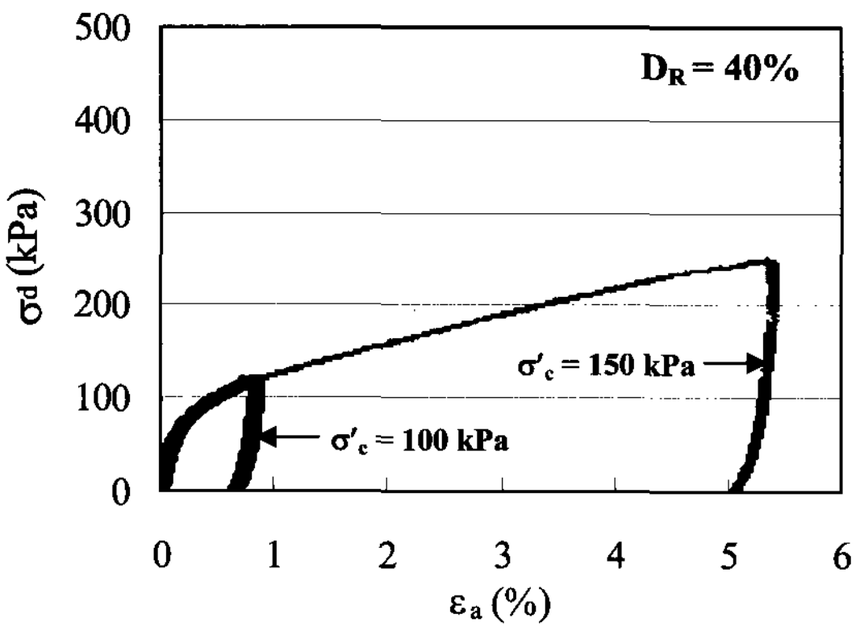


(a) $\sigma'_c$ = 100 and 150 kPa with $D_R$ = 40%

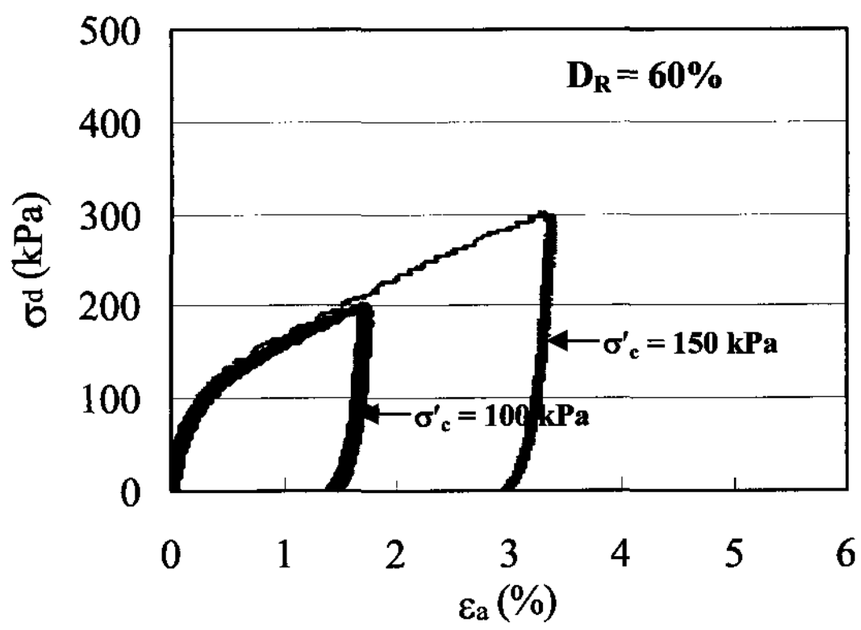


(b) $\sigma'_c$ = 100 and 150 kPa with $D_R$ = 60%

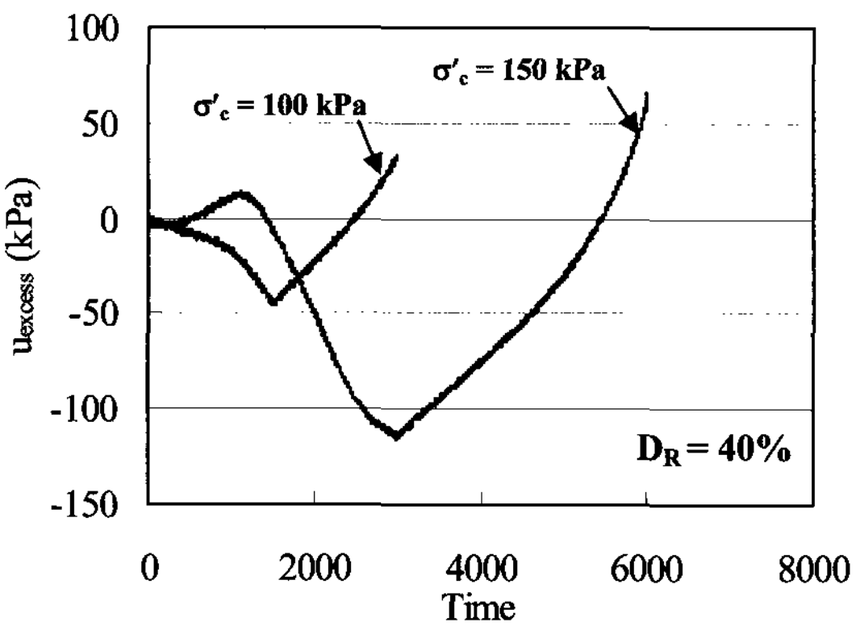


(c) $\sigma'_c$ = 100 and 150 kPa with $D_R$ = 40%

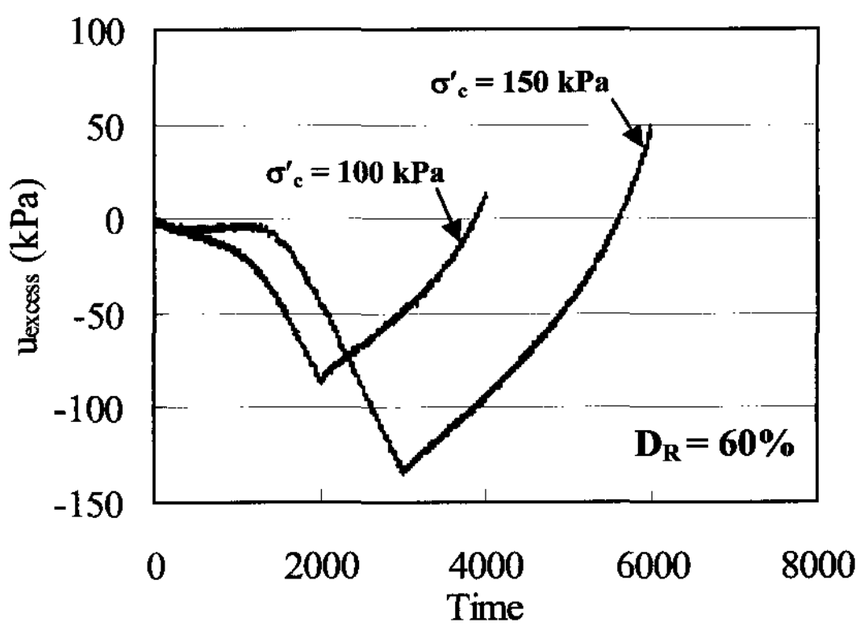


(d) $\sigma'_c$ = 100 and 150 kPa with $D_R$ = 60%

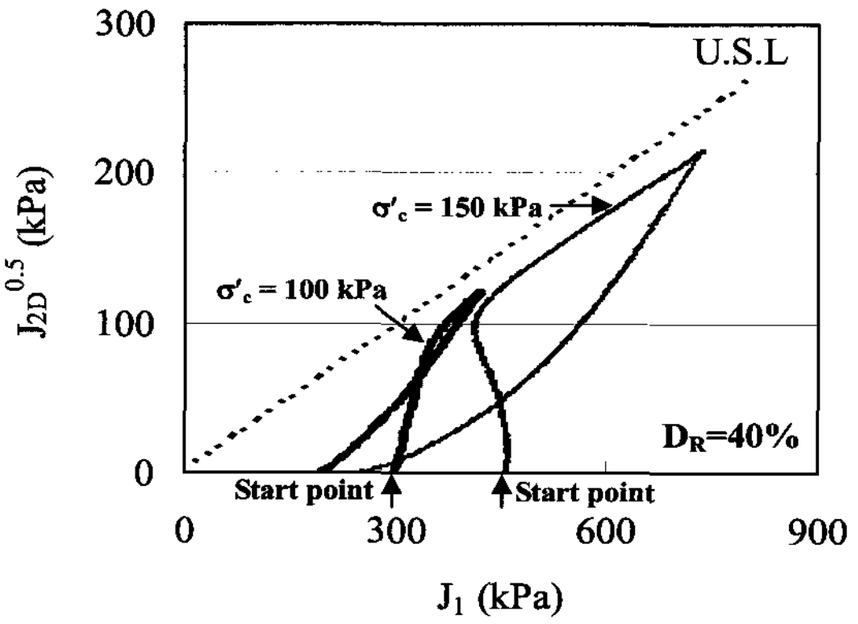


(e) $\sigma'_c$ = 100 and 150 kPa with $D_R$ = 40%

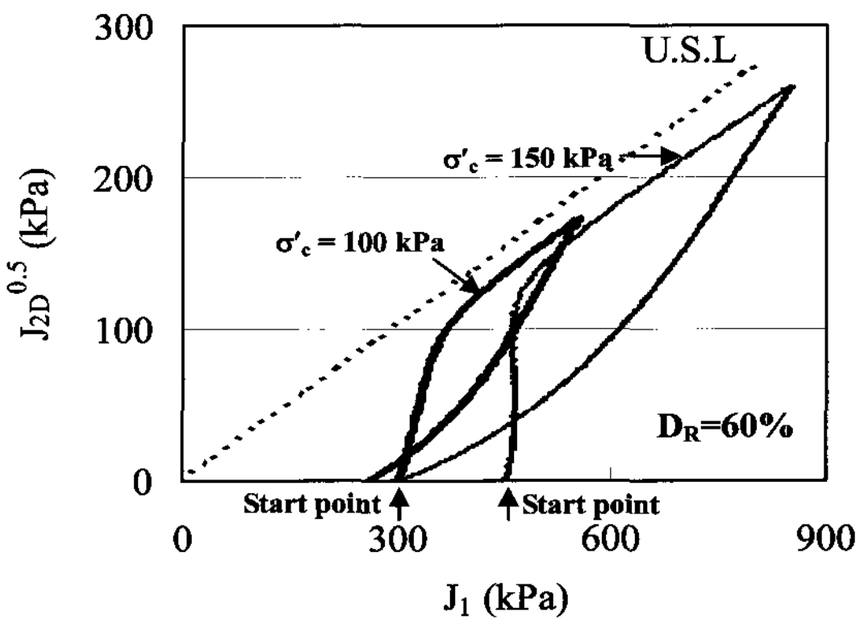


(f) $\sigma'_c$ = 100 and 150 kPa with $D_R$ = 60%

Fig. 5. Stress-strain curves and effective stress paths from static triaxial tests

the excess pore pressures are plotted against time. From this result, the excess pore pressures observed during loading are decreasing with time. The excess pore pressures increase obviously during unloading. Stress paths for the tests are shown in Figs. 5 (e) and (f). The straight lines plotted in the figures represent estimated ultimate state lines described previously. Slopes of the ultimate state lines appear to be virtually the same for both cases since those are the intrinsic soil variable that is unique for a given soil irrespective of density and stress states. It should be noticed that estimated ultimate state lines in Figs. 5 (e) and (f) may not be true ultimate state lines as further stress hardening appears to be possible as shown in Figs. 5 (a) and (b).

Fig. 6 shows stress-strain curves, mobilization of excess pore pressures, and stress paths obtained from cyclic triaxial tests. The characteristic hysteresis loops are generated by plotting the deviatoric stress versus the strain, acting on the sample and are shown in Figs. 6 (a) and (b). The loops tend to grow up progressively as the sample begins

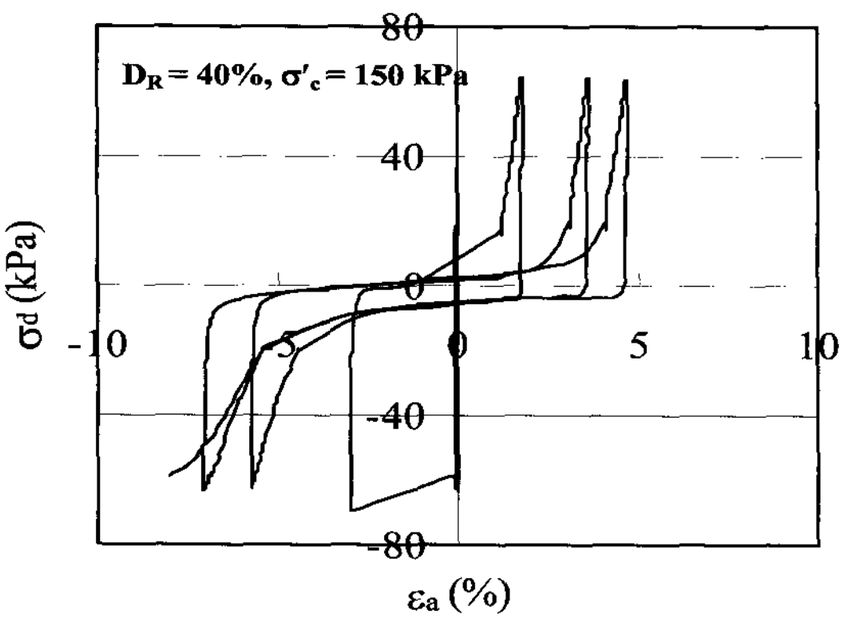


(a) $\sigma'_c$ = 150 kPa with $D_R$ = 40%

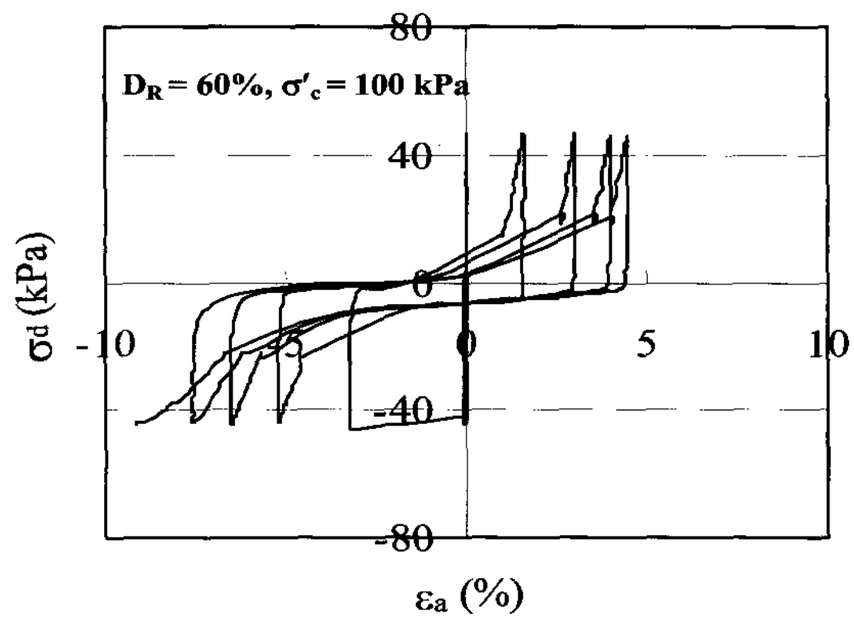


(b) $\sigma'_c$ = 150 kPa with $D_R$ = 60%

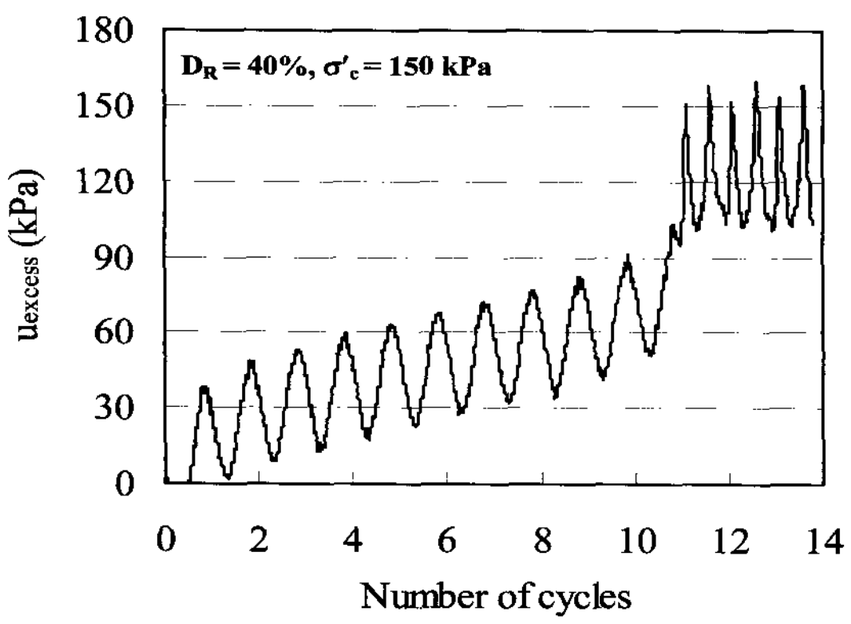


(c) $\sigma'_c$ = 150 kPa with $D_R$ = 40%

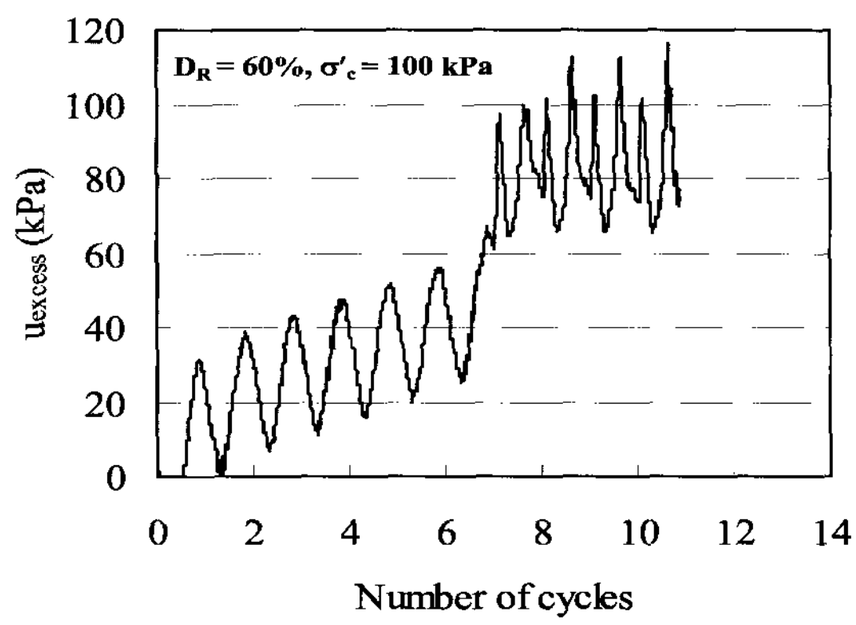


(d) $\sigma'_c$ = 150 kPa with $D_R$ = 60%

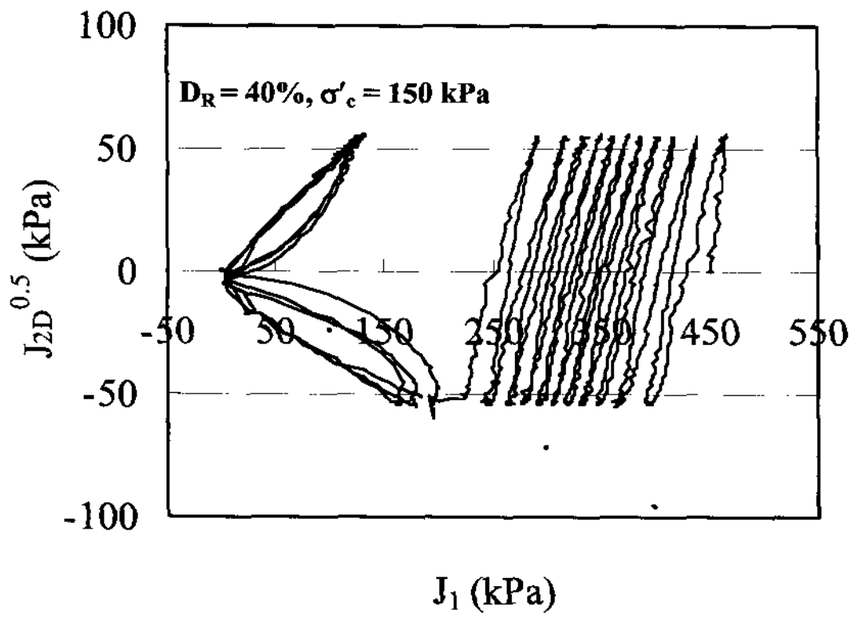


(e) $\sigma'_c$ = 150 kPa with $D_R$ = 40%

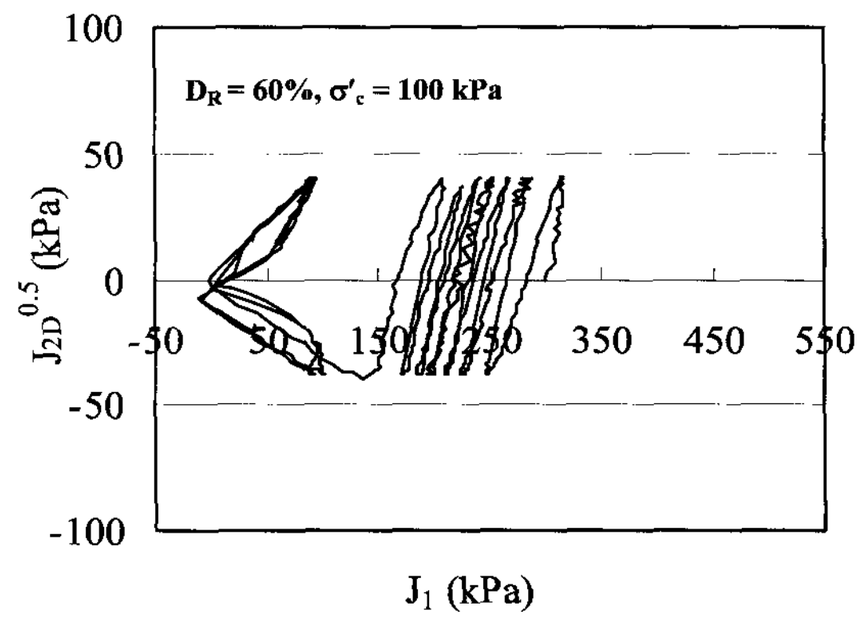


(f) $\sigma'_c$ = 150 kPa with $D_R$ = 60%

Fig. 6. Stress-strain curves, excess pore pressure development, and effective stress paths from static triaxial tests

to liquefy; after liquefaction the curves are maintained. As shown in Figs. 6 (c) and (d), the excess pore pressure continuously builds up until a certain number of loading cycles [i.e., N = 11 and 7 in Figs. 6 (c) and (d)], and then a rapid increase and oscillation of the excess pore pressure at a value approximately equal to the initial confining stress is observed. This can also be seen in effective stress paths shown in Figs. 6 (e) and (f). As shown in the figures, effective stress paths degrade gradually as the number of loading cycles increases. Once the effective stress path meets a certain point, it moves linearly to the origin of the zero effective stress state, after which oscillation with no average shear resistance is observed. This point, at which the linear stress degradation initiates, therefore, can be defined as the initial liquefaction occurrence.

## 4. Liquefaction Analysis Based on Dsc Model

### 4.1 Determination of Initial Liquefaction

Determination of the initial liquefaction is important as it defines the liquefaction resistance for a given soil against a given earthquake. According to Iai et al. [1992], the initial liquefaction can be defined from the liquefaction front state in terms of the plastic shear work, which can be obtained from cyclic stress-strain curves. This is based on the assumption that the excess pore pressure is also related to the plastic shear work. When a value of the plastic shear work, normalized with total plastic shear work at liquefaction, reaches 1.0 or the liquefaction front parameter defined by a current effective stress is smaller than 0.4, the dynamic effective stress path is found to move rapidly toward the zero effective stress state with initiation of liquefaction.

Other common approach for the determination of the initial liquefaction is based on the flow liquefaction surface [Vade and Chern, 1983]. The flow liquefaction surface can be obtained at the phase change state toward the ultimate or steady state on effective stress paths of undrained static triaxial tests. The flow liquefaction surface, therefore, represents the same definition as the phase change line described in the DSC model.

For the application of the disturbed state concept to liquefaction, Desai et al. [1998] suggested that the initiation of liquefaction is closely related to the critical disturbance $D_c$, which corresponds to the maximum curvature point on the disturbance function curve shown in Fig. 2 (b). This is based on experimental observation that the number of loading cycles to reach $D_c$ approximately matches that required to reach the initial liquefaction. According to Desai et al. [1998], the critical disturbance $D_c$ is determined from the optimized disturbance function curve in terms of the disturbance D and the deviatoric plastic trajectory $\xi_D$ drawn at every single loading cycle. This indicates that values of $D_c$ from the original DSC model may not exactly coincide with actual liquefaction initiations as detailed components of a single loading cycle from compression to tension are not reflected. In the present study, therefore, the determination of the critical disturbance $D_c$ and the initial liquefaction is based on the effective stress path with more detailed loading components. In particular, the phase change line is introduced to define the critical disturbance and the initial liquefaction. Comparison between different definitions for the initial liquefaction will be further discussed.

Fig. 7 shows phase change (PCL) and ultimate state lines (USL) obtained from effective stress paths for both static and cyclic triaxial tests. For cyclic triaxial tests shown in Figs. 7 (c) and (d), phase change lines were defined as a line between the origin and the initial liquefaction point corresponding to a point at which the rapid decrease of effective stress initiates [i.e., PCP in Figs. 7 (c) and (d)]. In the present study, the phase change line obtained from cyclic tests is referred to as the dynamic phase change line (DPCL). From Fig. 7, it is seen that the phase change line and the dynamic phase change line obtained from static and cyclic triaxial tests are virtually the same, whereas the determination procedure and mechanical features of the two tests are different. It is also seen that, after the initial liquefaction at the dynamic phase change line from cyclic triaxial test, there is another line (DUSL) along which the stress paths show a cyclic regularity. This line was found to be similar to the ultimate

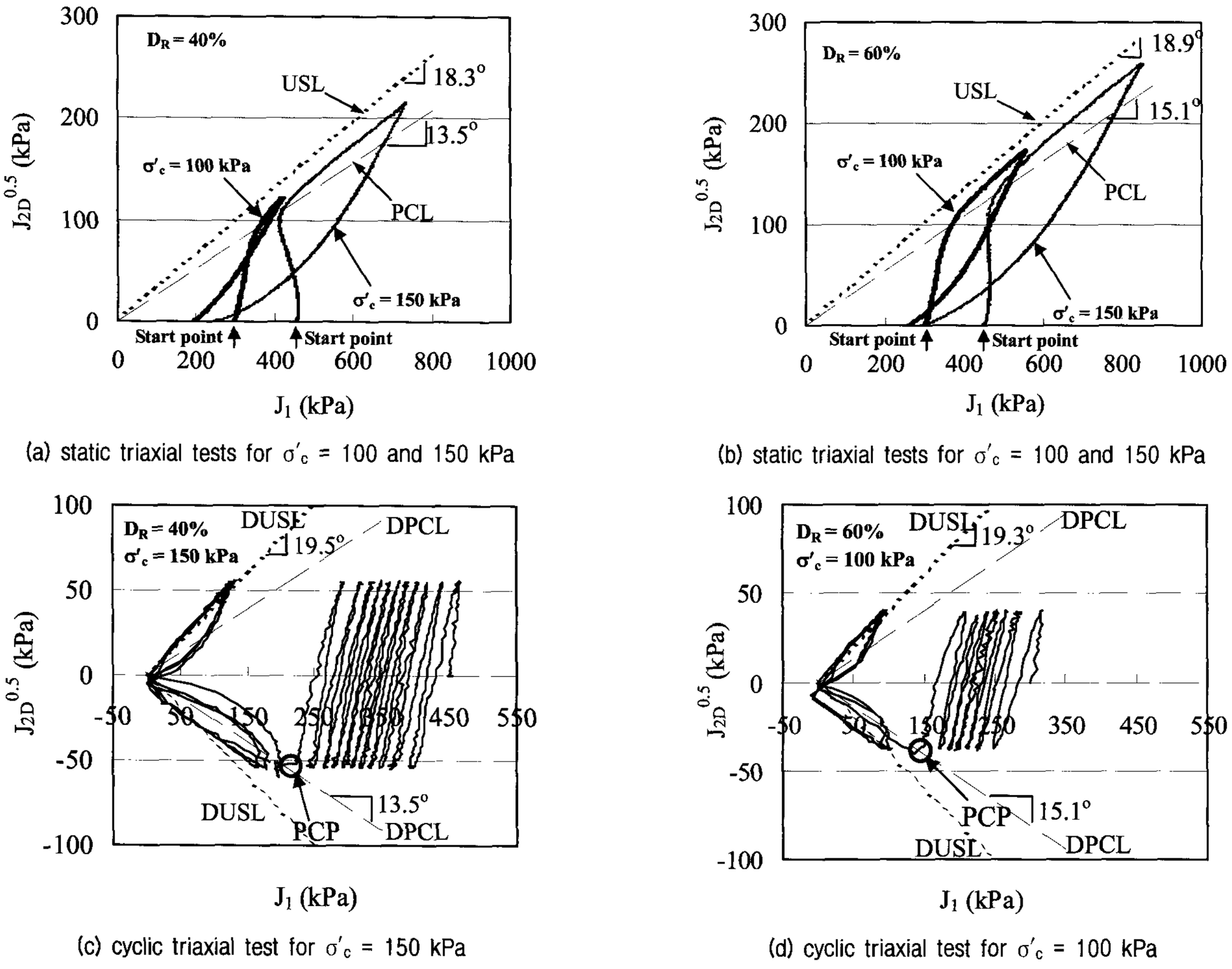


Fig. 7. Phase change and ultimate state lines based on effective stress paths

state line observed from static triaxial tests. The consistency of the phase change and ultimate state lines from both tests is reasonable as all the test results are based on effective stresses. This result also indicates that a single cyclic triaxial test can provide significant soil parameters required for liquefaction analysis using DSC model.

## 4.2 Classification of Dynamic Soil Phases and Modified DSC Model

From cyclic triaxial test results, it was found that the effective stress path under dynamic loading conditions consists of three different phases: gradual degradation of effective stress, initial liquefaction with rapid stress degradation, and fully developed liquefaction. The gradual degradation phase of effective stress corresponds to the unstable state under which significant deformations develop, while the fully developed liquefaction phase represents the ultimate state with no further shear resistance available. The initial liquefaction is defined as a stage from which rapid development of the excess pore pressure occurs with an effective stress path moving towards the zero-effective stress state along the phase change line. Fig. 8 shows different phases of dynamic soil responses and corresponding excess pore pressure development. As shown in the figure, the excess pore pressure accumulates continuously during the gradual degradation phase of effective stress and then rapid increase and full development of the excess pore pressure are observed at the initial liquefaction and fully developed liquefaction phases, respectively.

In the original DSC model [Desai et al., 1998], liquefaction is defined to initiate at a certain number of loading cycles corresponding to the critical disturbance $D_c$ obtained from the optimized disturbance function curve. For small strain problems before failure, such as dynamic responses of axially-loaded pile, this approach has been successfully implemented [Desai and Rigby, 1997; Pal and Wathugala,

1999]. For the analysis of initiation and full development of liquefaction, however, this approach has not been fully verified as it does not include detailed variations of dynamic soil phases described in Fig. 8. In this study, therefore, a modification was made into the original DSC model such that initial liquefaction occurrence and different soil phases are defined in terms of the phase change and ultimate state lines from dynamic effective stress paths. This modification reflects more detailed dynamic soil responses and actual liquefaction initiation observed from experimental test results. As discussed earlier, both phase change and ultimate state lines required in this modification can be obtained from a single cyclic triaxial test.

The FA state in the original DSC model is defined by the critical state model [Roscoe et al., 1958]. In the modified DSC model, the FA state is defined by Drucker-Prager model [1952] for which the failure envelope can be determined from the ultimate state line of the cyclic effective stress path. This modification represents a much simpler procedure for the parameter determination than the original DSC as a single cyclic triaxial test provides key parameters for both RI and FA states. The disturbance D from the modification is then defined as follows:

$$D = \frac{J_1^R - J_1^O}{J_1^R - J_1^F} \tag{8}$$

where $J_1^R$, $J_1^F$, and $J_1^a$ are the first stress invariants for RI, FA, and observed states, respectively.

In the original DSC model [Desai et al., 1998], values of the disturbance D are obtained at every single cycle in the cyclic loading process. In the new procedure for the modified DSC model, values of D are obtained at every 1/4 cycle of compression, unloading, extension, and

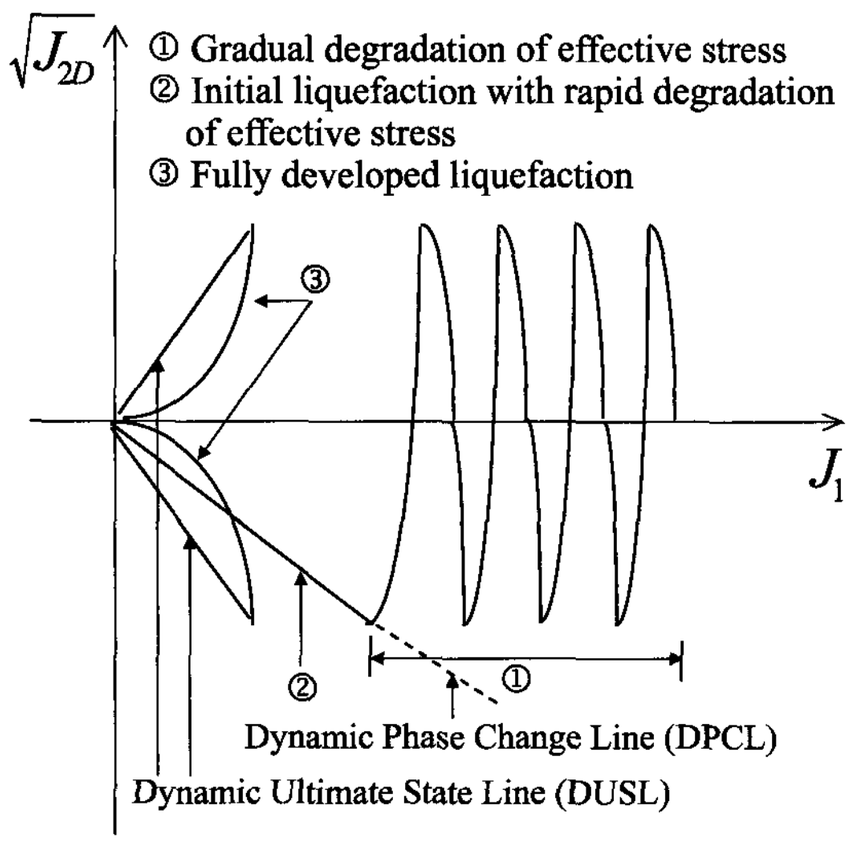


(a) dynamic effective stress path

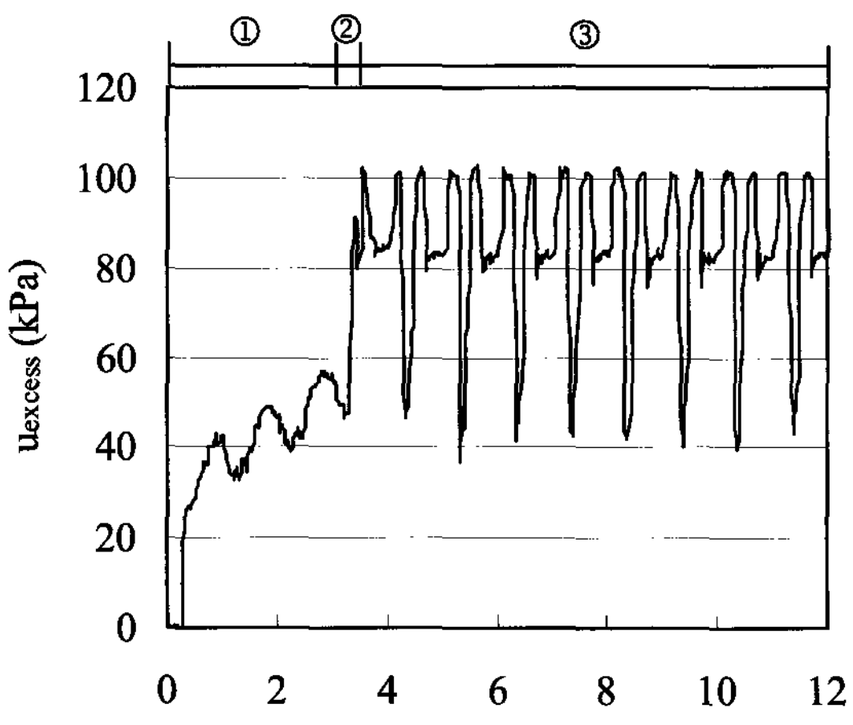


(b) excess pore pressure development

Fig. 8. Classification of dynamic soil phases

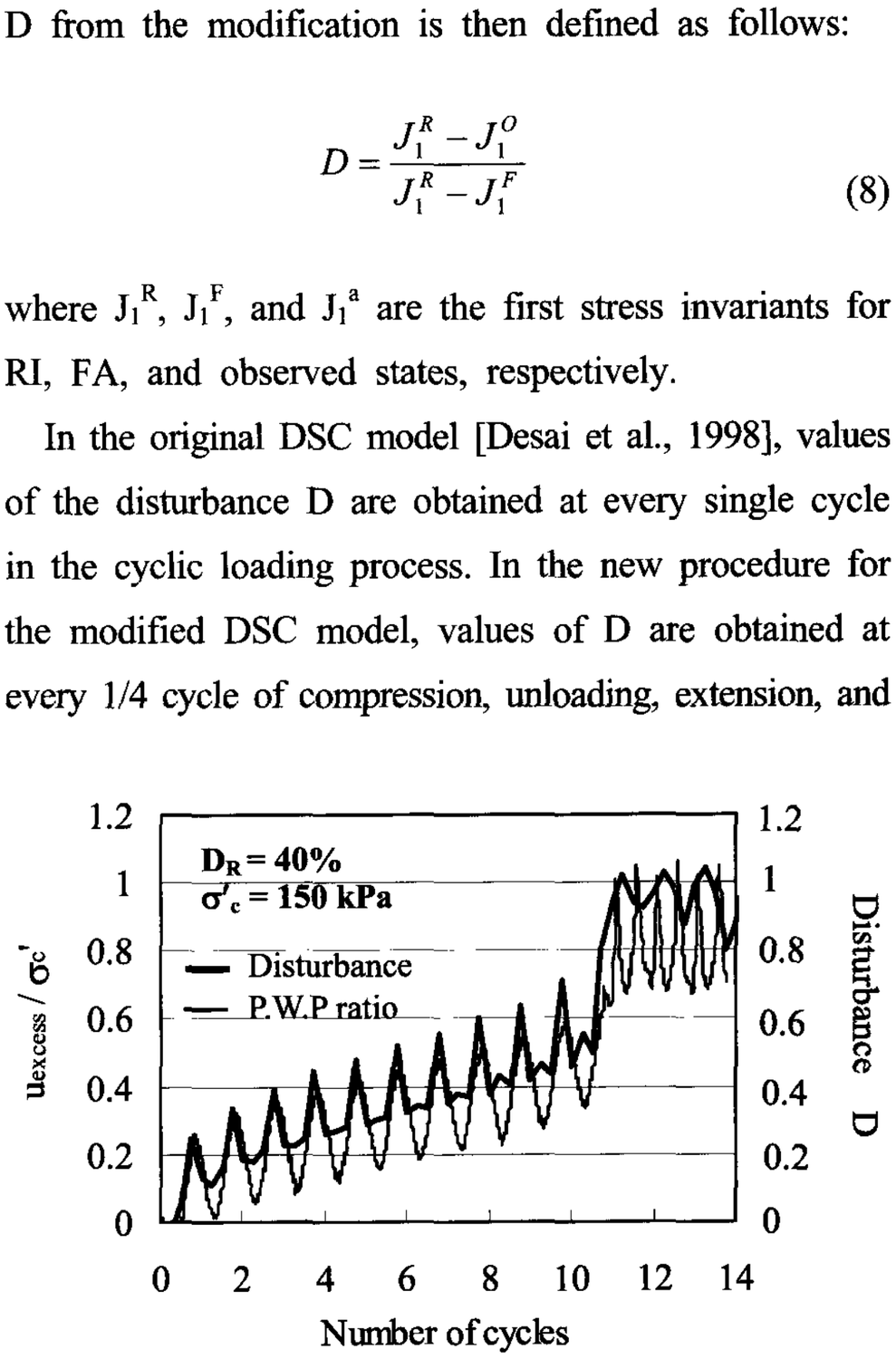


(a) $\sigma'_c$ = 150 kPa and $D_R$ = 40%

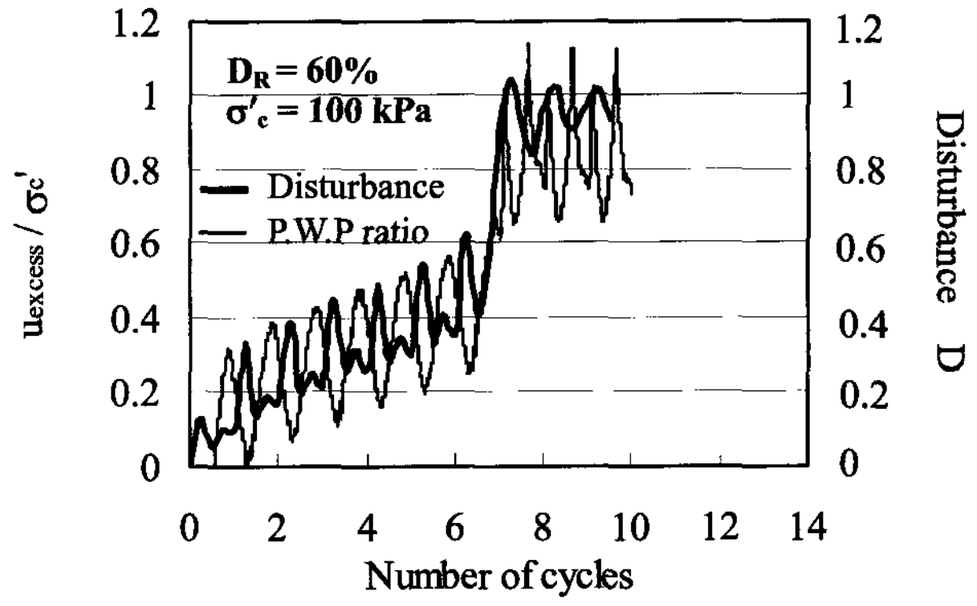


(b) $\sigma'_c$ = 100 kPa and $D_R$ = 60%

Fig. 9. Excess pore pressure ratios and disturbances with number of loading cycles

unloading phases for a given loading cycle. This aims at describing more realistic and detailed liquefaction behavior as the use of a single cycle may not detect the specific point at which significant changes of the excess pore pressure occur as a liquefaction initiation point.

Fig. 9 shows values of the disturbance D based on Eq. (8) and excess pore pressures ratio $u_{excess}/\sigma'_c$ plotted at every 1/4 loading cycle. As can be seen in Fig. 9, changes of D with number of loading cycles appear to be nearly identical to the mobilization of the excess pore pressure. Results in Fig. 9 suggest that the disturbance D can be effectively used for the description of the excess pore pressure development and thus as an index for the assessment of liquefaction potential.

### 4.3 Determination of Deviatoric Plastic Strain Trajectory

The deviatoric plastic strain trajectory $\xi_D$ for the initial liquefaction in the original DSC model is obtained from $D_c$ corresponding to the maximum curvature point on the optimized disturbance function curve. Curvature of the optimized disturbance function curve is given by:

$$R = \frac{D''}{\left(1 + D'^{\,2}\right)^{3/2}} \tag{9}$$

where R = curvature of the disturbance function curve given by (4); and D′ and D″ = the first and second derivatives of the disturbance function with respect to $\xi_D$. Detailed formulation of D′ and D″ are:

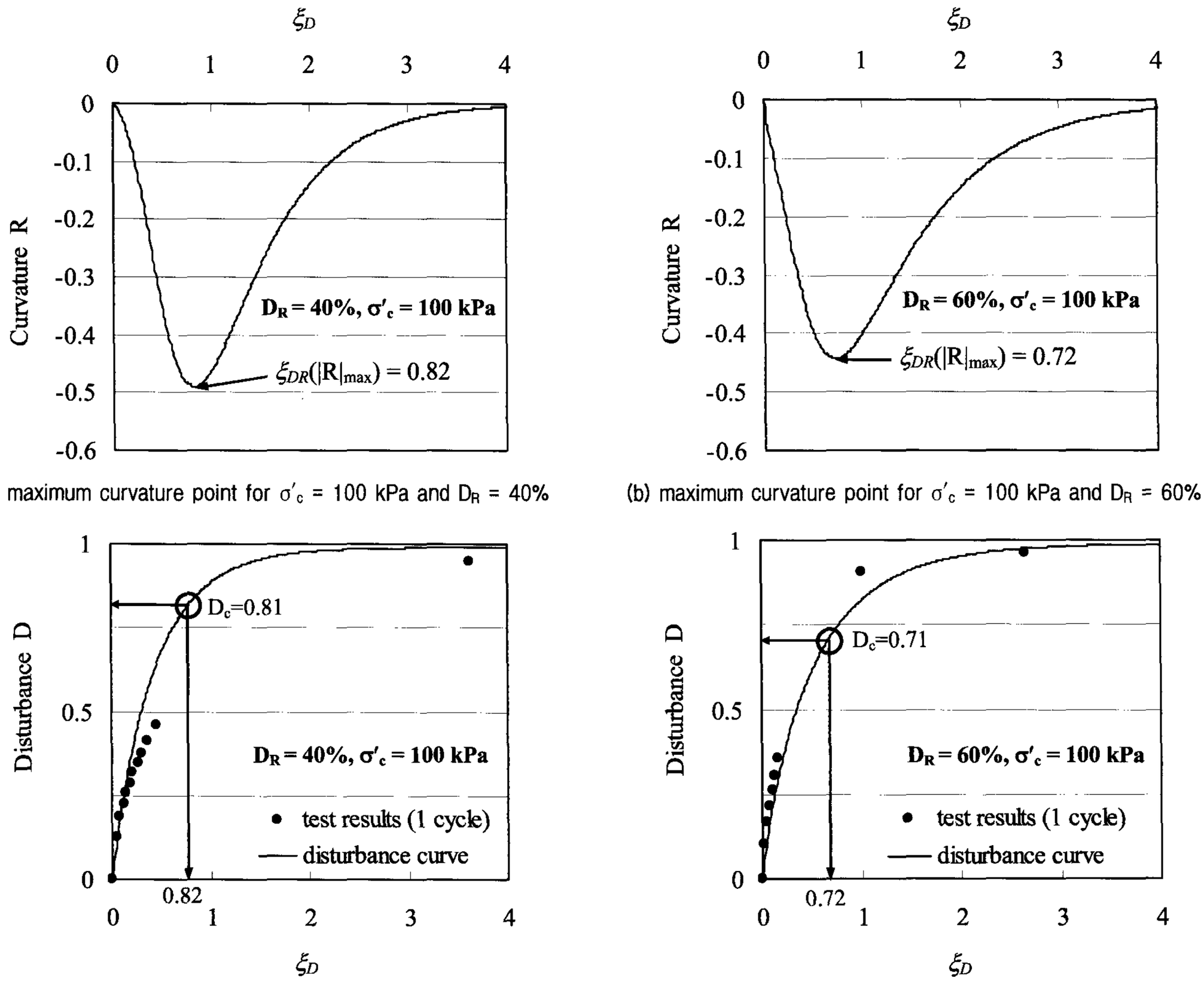


(a) maximum curvature point for $\sigma'_c$ = 100 kPa and $D_R$ = 40%

(b) maximum curvature point for $\sigma'_c$ = 100 kPa and $D_R$ = 60%

(c) determination of $D_c$ for $\sigma'_c$ = 100 kPa and $D_R$ = 40%

(d) determination of $D_c$ for $\sigma'_c$ = 100 kPa and $D_R$ = 60%

Fig. 10. Determination of Dc from original DSC model

$$D' = \frac{dD}{d\xi_D} = 0.99 \times (AZ)\xi_D^{Z-1} Exp\left(-A\xi_D^Z\right) \quad (10)$$

$$D'' = \frac{d^2D}{d\xi_D{}^2} = 0.99 \times (AZ)\xi_D^{Z-2} Exp\left(-A\xi_D^Z\right)\left[Z - 1 - AZ\xi_D^Z\right] \quad (11)$$

where A and Z = material constants. Fig. 10 shows calculation of D and $\xi_D$ for the original DSC model using the cyclic triaxial test results presented previously. Fig. 11 shows values of the critical disturbance $D_c$ and corresponding deviatoric plastic trajectory $\xi_D$ obtained from (5) and effective stress paths for the proposed method. Comparing results in Figs. 10 and 11, it is observed that the original DSC approach produces higher values of $\xi_D$ than those obtained from the modified DSC approach. This in turn indicates that the liquefaction resistance for a given soil from the original DSC model may be overestimated, which is unconservative.

## 4.4 Calculated and Observed Cyclic Soil Responses

For the application of the DSC model to liquefaction, numerical codes based on the incremental integral scheme for both the original and modified DSC models were developed and used in the comparison with experimental test results. In the modified DSC model, the RI state was defined with the HiSS model by Desai et al. [1991] as in the original DSC model, while the Drucker-Prager model [1952] was employed for the FA state. For the original DSC model [Desai et al., 1998], dynamic soil responses and initiation of liquefaction were defined in terms of the critical disturbance $D_c$ obtained at the maximum curvature point on the optimized disturbance function curve. The modified DSC model, on the other hand, includes different soil phases of the gradual stress degradation, initial liquefaction, and fully developed liquefaction,

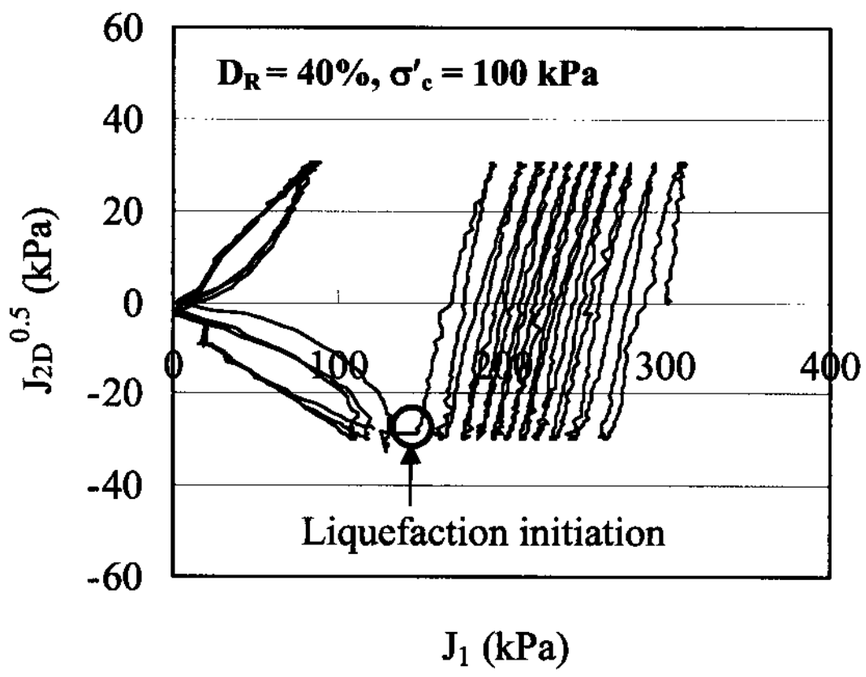


(a) liquefaction initiation point from cyclic effective stress path for $\sigma'_c$ = 100 kPa and $D_R$ = 40%

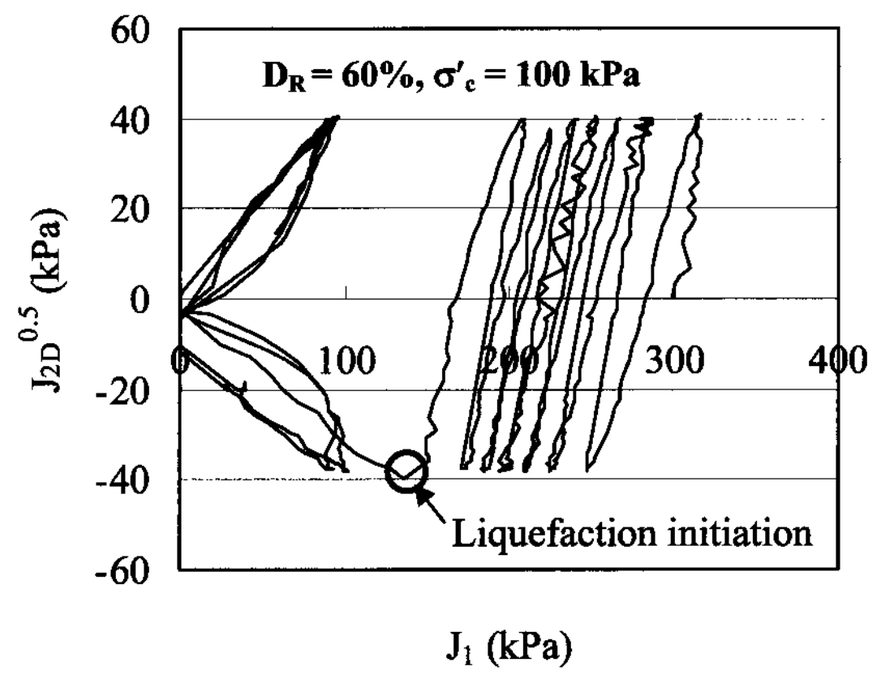


(b) liquefaction initiation point from cyclic effective stress path for $\sigma'_c$ = 100 kPa and $D_R$ = 60%

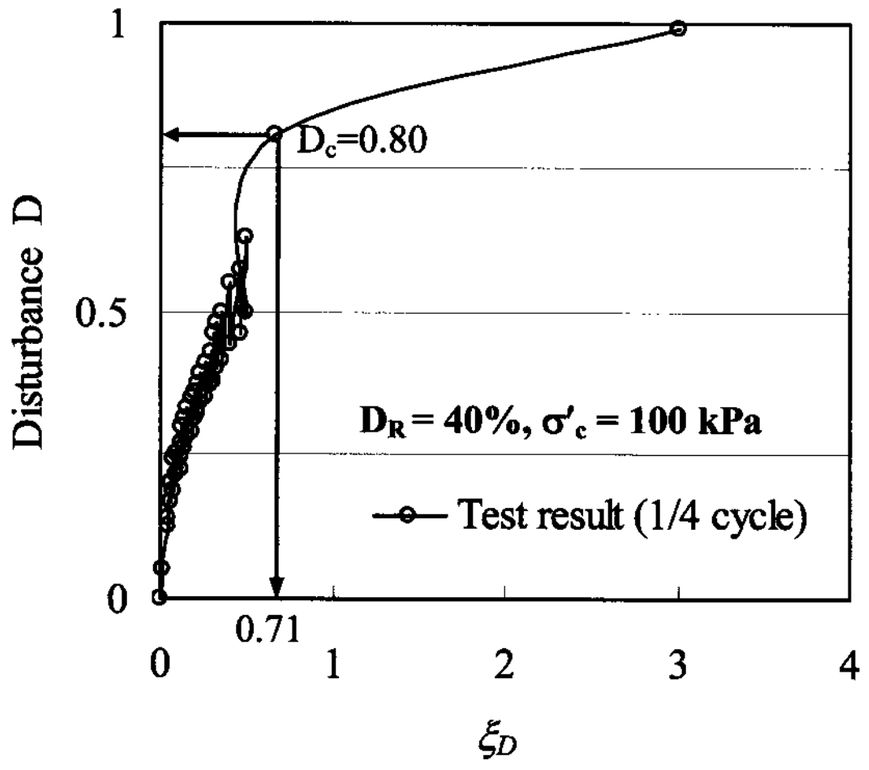


(c) determination of $D_c$ for $\sigma'_c$ = 100 kPa and DR = 40%

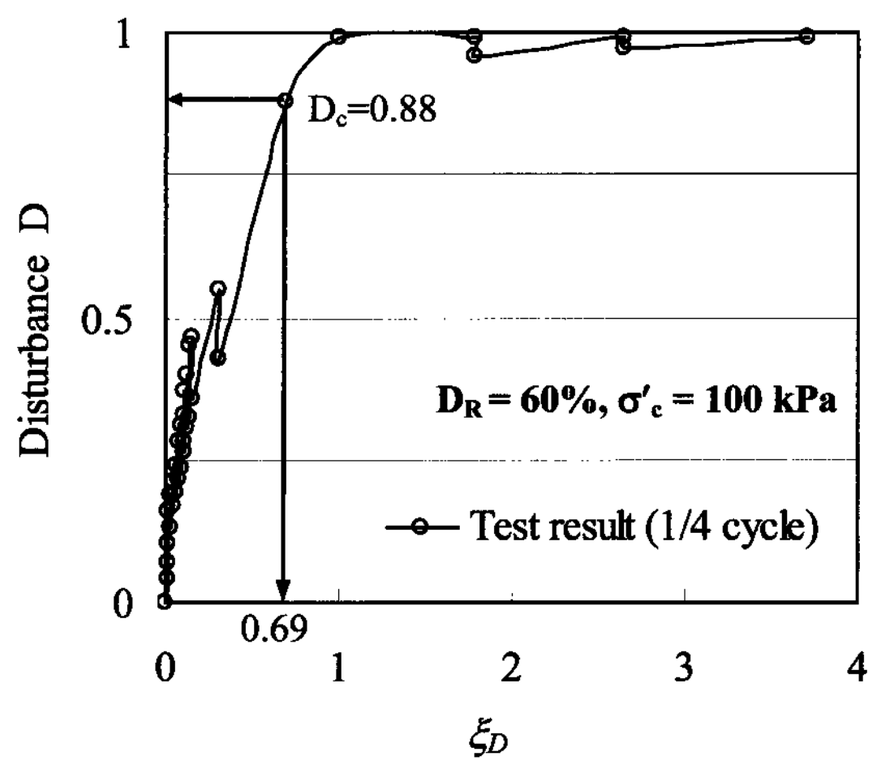


(d) determination of $D_c$ for $\sigma'_c$ = 100 kPa and DR = 60%

Fig. 11. Determination of $D_c$ from modified DSC model

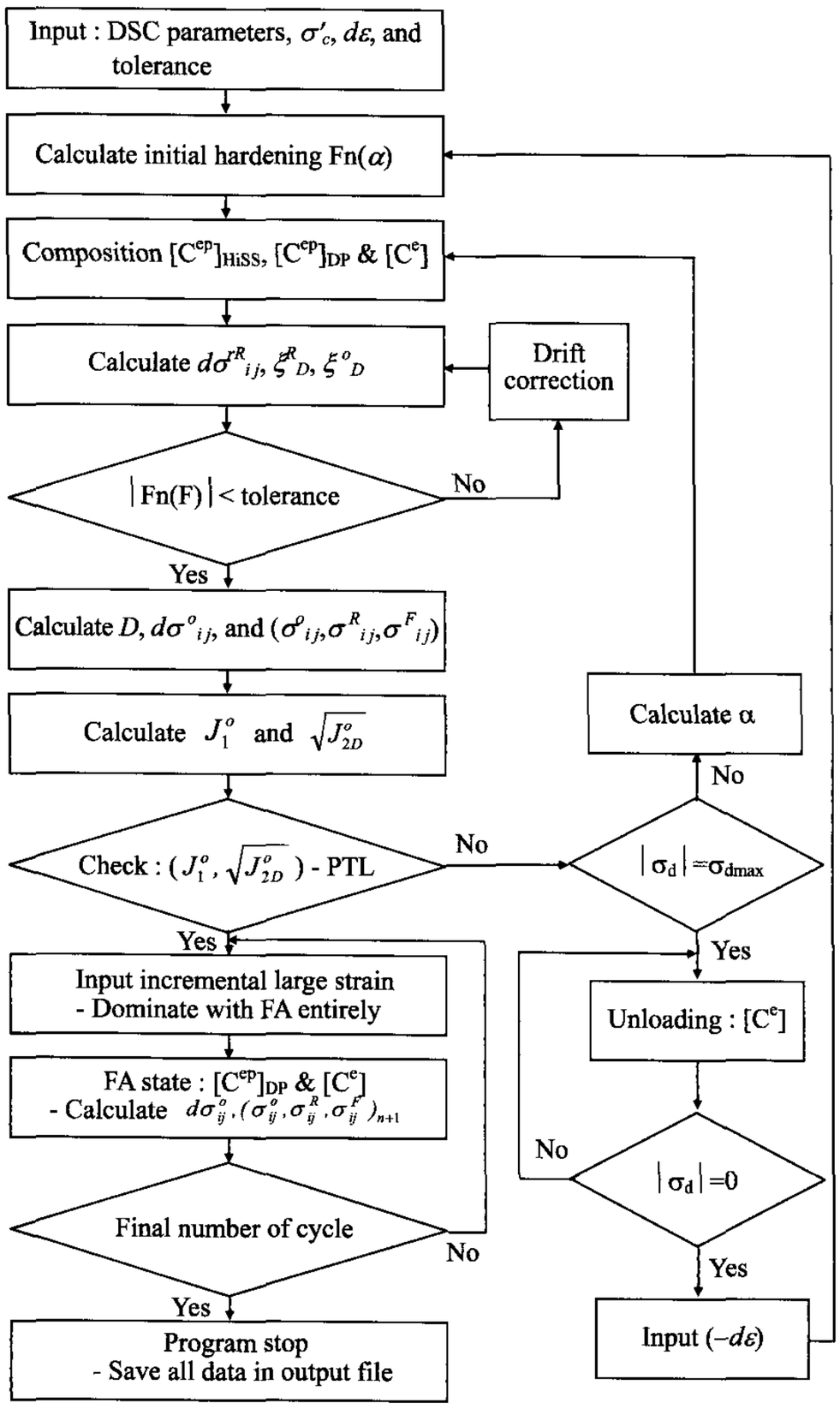


Fig. 12. Computation procedure for modified DSC model

based on the dynamic phase change and ultimate state lines shown in Figs. 7 and 8. Fig. 12 shows the computation procedure of the program developed for the modified DSC model.

The DSC and modified DSC model involves a number of material constants and they can be determined from a series of static and cyclic triaxial test results. The material constants can be divided into four categories: the elastic state parameters, the plastic state parameters, the ultimate state parameters, and the parameters for describing disturbance function. The elastic state parameters E and ν are found from the slopes of unloading parts of the strain-stress curves (Fig. 6). The parameters for the plastic state $\gamma_u$ and β are associated with the ultimate state, which is defined as the locus of the stress states asymptotic to the observed stress-strain curve. To find the plastic state parameters $\gamma_u$ and β, which are related to the slope of the ultimate envelope in $J_{2D}{}^{0.5}$ - $J_1$ space, at least two different stress paths are required. The phase change parameter, n is the parameter related to the point at which the plastic volume change is zero. Fig. 7 shows phase change (PCL) obtained from effective stress paths for both static and cyclic triaxial tests. Therefore, the parameter n is calculated by Fig. 7 and Eq. (6). Values of the model parameter $h_1$ and $h_2$ in Eq. (7) can be estimated from the

Table 2. Input parameters used in calculation

| | Original DSC model | | | Modified DSC model | | |
|---|---|---|---|---|---|---|
| | | $D_R$ = 40% $\sigma'_c$ = 150 kPa | $D_R$ = 60% $\sigma'_c$ = 100 kPa | | $D_R$ = 40% $\sigma'_c$ = 150 kPa | $D_R$ = 60% $\sigma'_c$ = 100 kPa |
| Elastic state | E | 175 MPa | 210 MPa | E | 175 MPa | 210 MPa |
| | ν | 0.38 | 0.38 | | 0.38 | 0.38 |
| Plastic State | $\gamma_u$ | 0.25 | 0.25 | $\gamma_u$ | 0.25 | 0.25 |
| | | 0 | 0 | | 0 | 0 |
| | n | 2.80 | 2.67 | n | 2.80 | 2.67 |
| | $h_1$ | 0.059 | 0.152 | $h_1$ | 0.059 | 0.152 |
| | $h_2$ | 0.016 | 0.092 | $h_2$ | 0.016 | 0.092 |
| Ultimate State* | $\bar{m}$ | 0.5 | 0.5 | M | 0.5 | 0.5 |
| | λ | 0.045 | 0.052 | k | 0 | 0 |
| | $e_o^c$ | 0.636 | 0.0624 | – | – | – |
| Disturbance parameters | $D_u$ | 0.99 | 0.99 | $D_u$ | 0.99 | 0.99 |
| | A | 1.458 | 1.771 | A | 1.107 | 1.771 |
| | Z | 0.779 | 0.882 | Z | 0.671 | 0.882 |

* $\bar{m}$, λ, and $e_o^c$ = Critical state concept model parameters; M and k = Drucker–Prager model parameters

first-order polynomial regression line that is obtained by taking the natural log operator in both sides of Eq. (7). The slope and intercept of this line give the values of $h_1$ and $h_2$, respectively. The ultimate state parameters $\overline{m}$, M, $\lambda$, and $e_0^c$ are evaluated from the characteristics of the ultimate state line (USL), where, $\overline{m}$ and M are the slope of the USL in the $J_{2D}^{0.5}$ - $J_1$ space (Fig. 7). $e_0^c$ is the reference void ratio evaluated at a mean pressure ($J_1/3$) of 1 kPa. $\lambda$ is the slope of the USL in e - ln($J_1/3$) space. The disturbance parameters $D_u$, A, and B are evaluated from Eq. (4). For each test, the maximum value of the disturbance is found and an arithmetic average value $D_u$ is estimated from the values calculated for each test. The calculated D and $\xi_D$ together with $D_u$ are used to plot

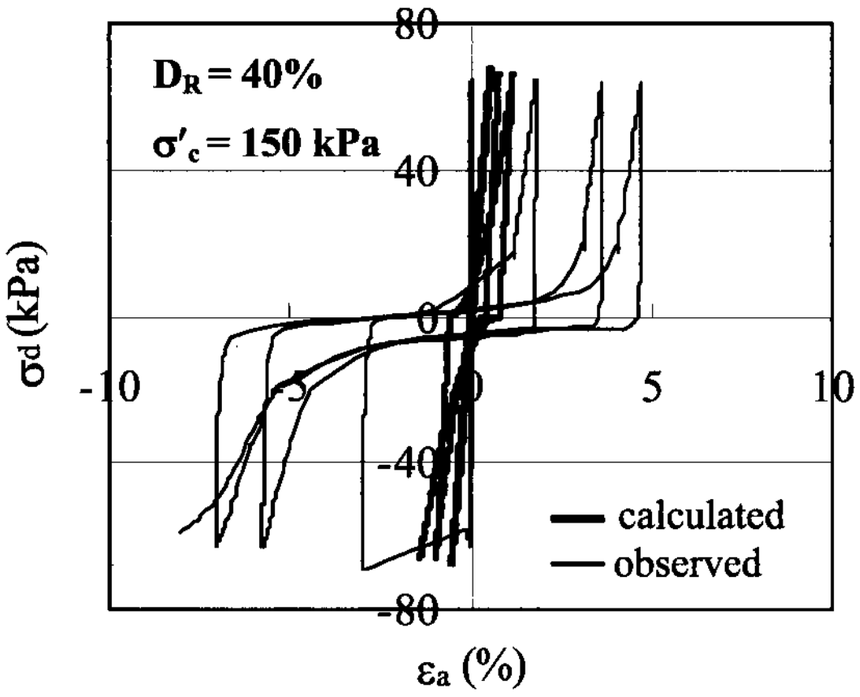


(a) stress-strain curves with $D_R$ = 40%

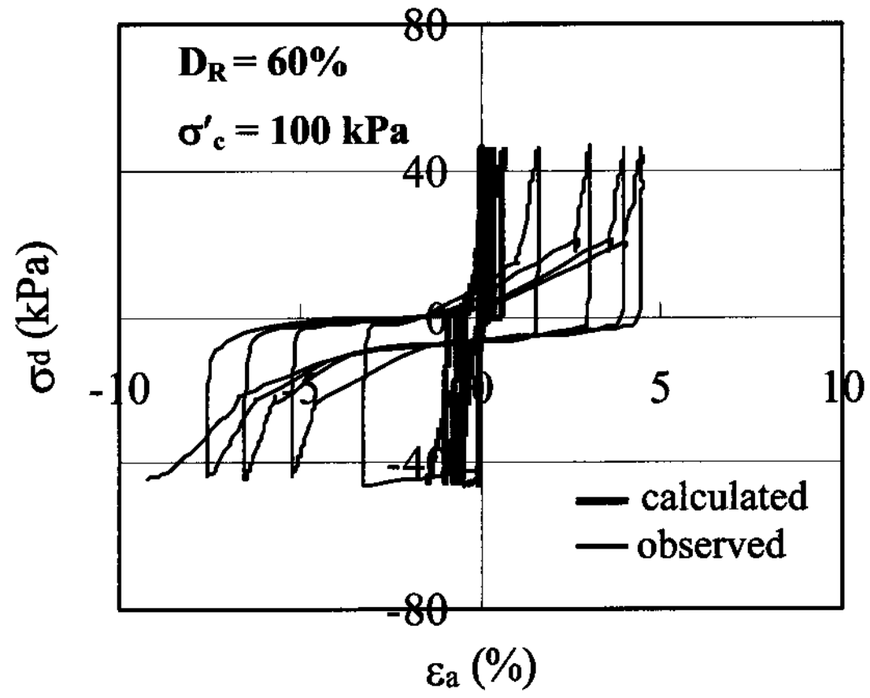


(b) stress-strain curves with $D_R$ = 60%

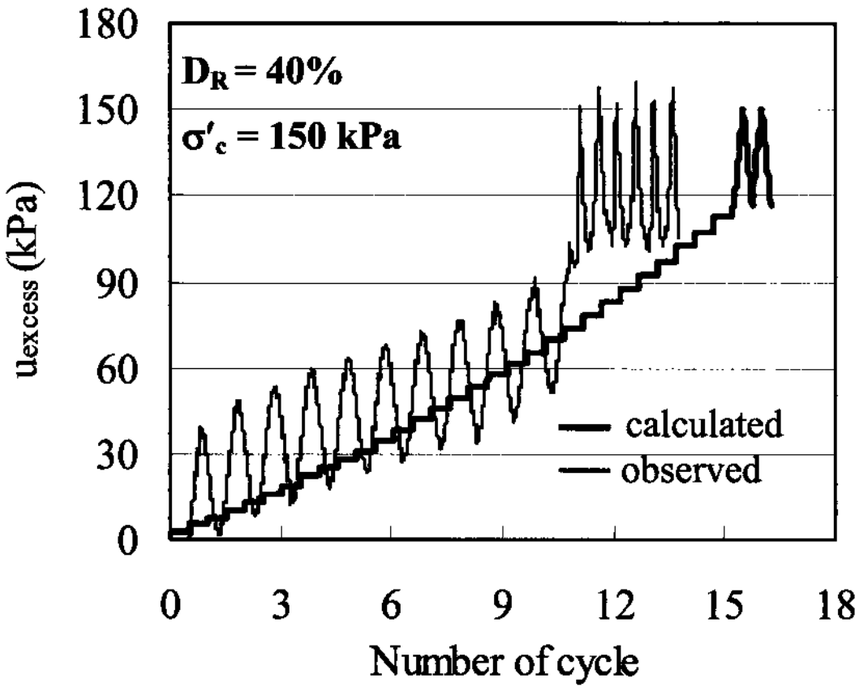


(c) excess pore pressure developments for $D_R$ = 40%

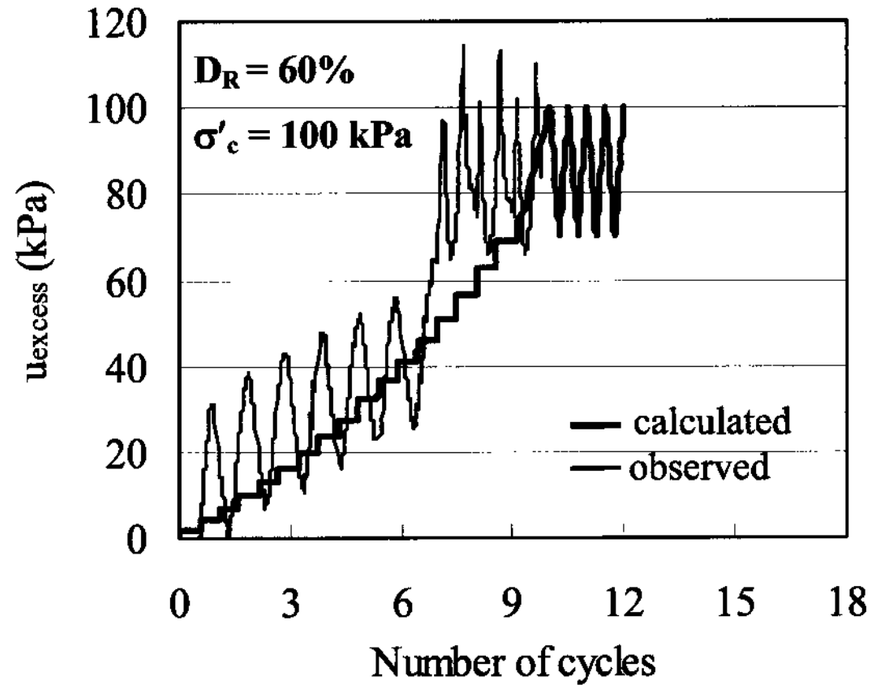


(d) excess pore pressure developments for $D_R$ = 60%

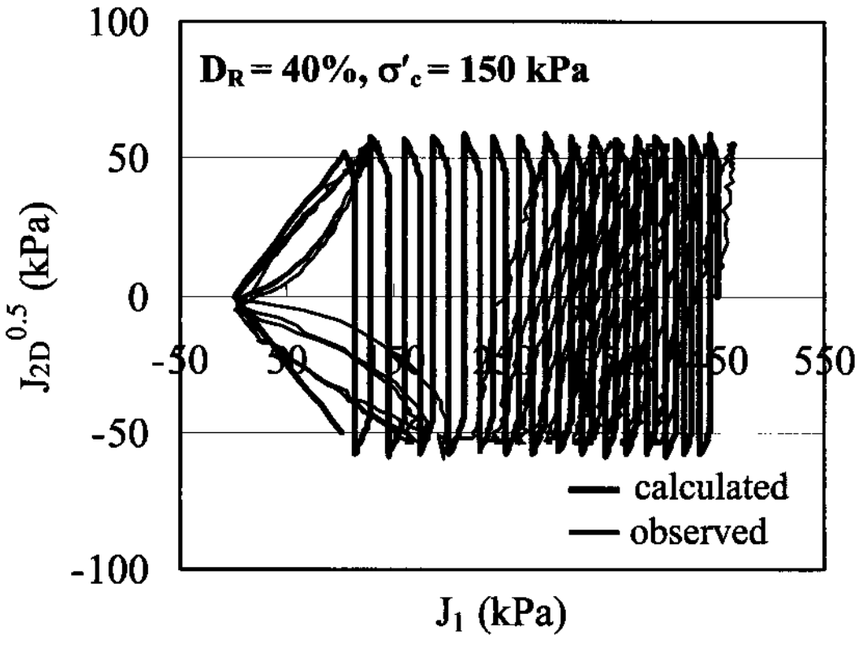


(e) effective stress paths for $D_R$ = 40%

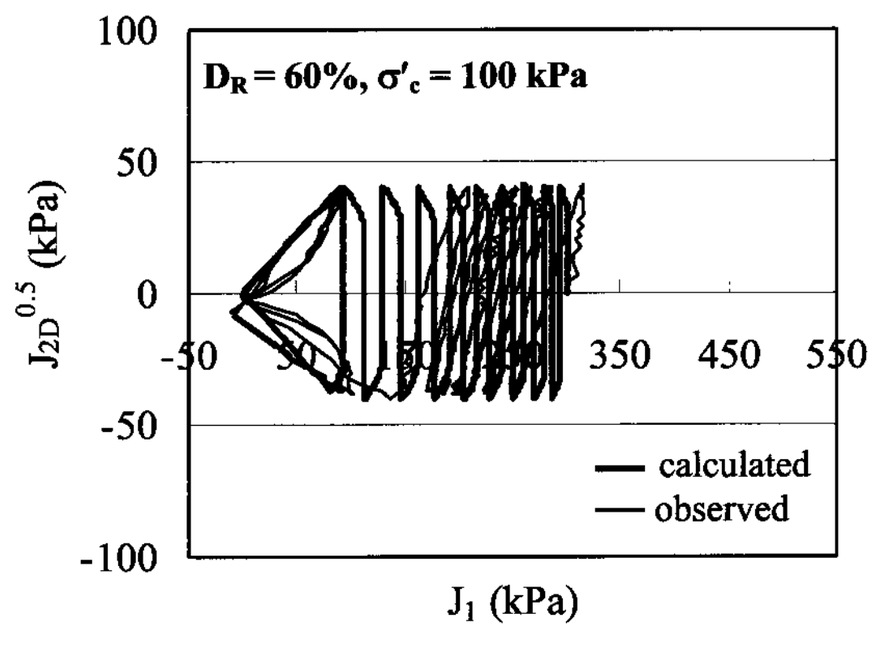


(f) effective stress paths for $D_R$ = 60%

Fig. 13. Calculated and observed cyclic soil responses with original DSC model

the data in $\ln[-\ln(\{D_u - D\}/D_u)] - \ln \xi_D$ space. Choosing an average straight line through the plotted data gives the A and Z values for the test under consideration. The input parameters were summarized in Table 2.

Figs. 13 and 14 show calculated and observed cyclic soil responses using the original and modified DSC models, respectively. As shown in Fig. 13, excess pore pressures and effective stress paths calculated from the original DSC represent overall agreement with observed results for the gradual degradation phase of effective stress. As the stress path approaches to the initial liquefaction stage, however, it is seen that the difference between calculated and observed results becomes more pronounced with different liquefaction initiation points. This result indicates that the critical disturbance $D_c$ obtained from the procedure of the original DSC model does not match well the actual

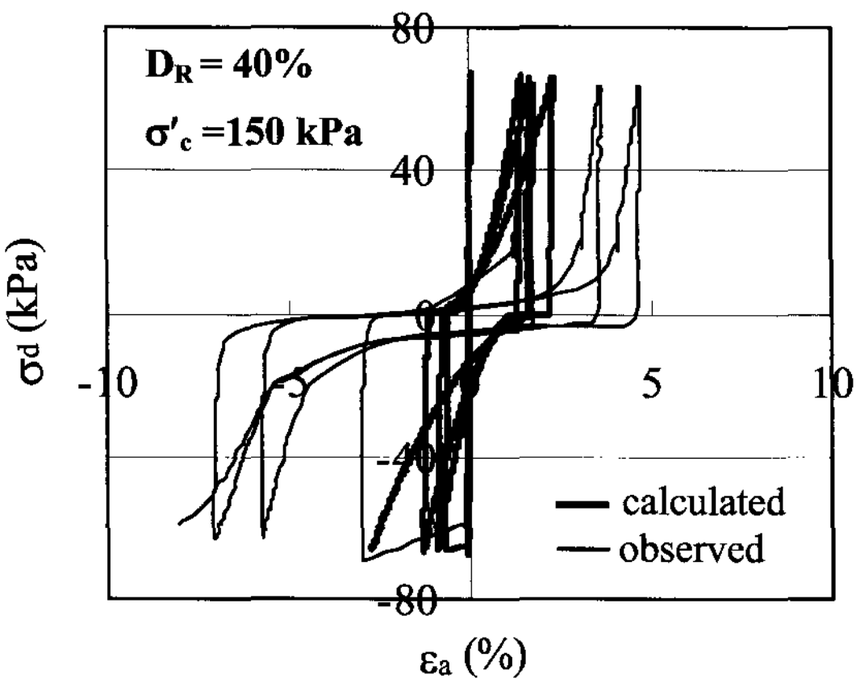


(a) stress-strain curves with $D_R$ = 40%

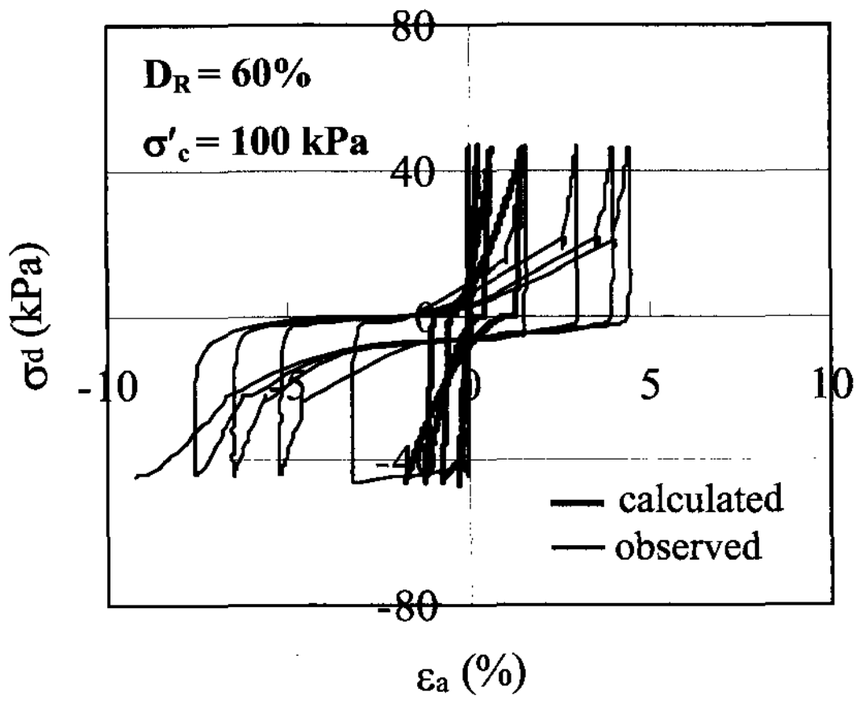


(b) stress-strain curves with $D_R$ = 60%

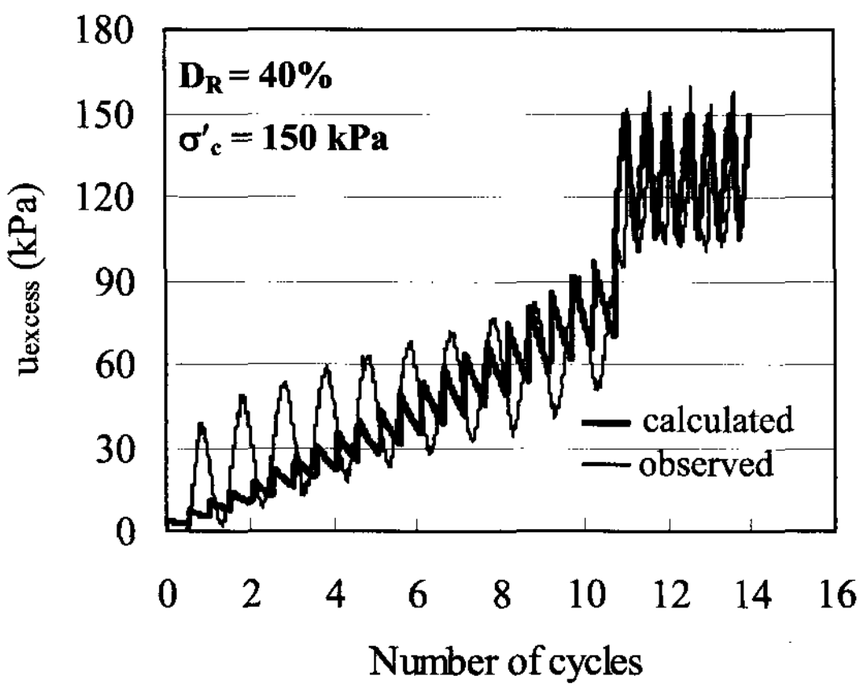


(c) excess pore pressure developments for $D_R$ = 40%

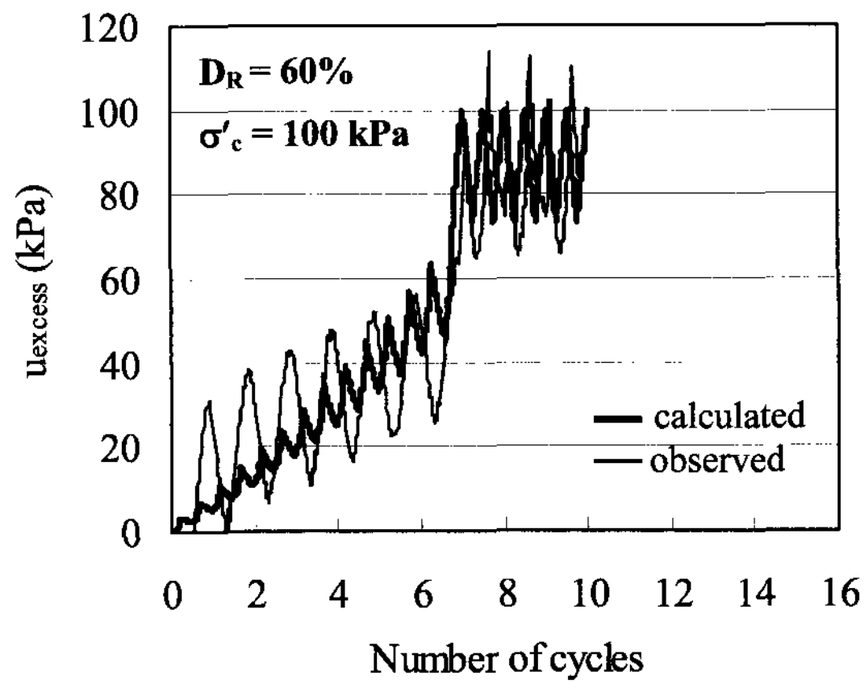


(d) excess pore pressure developments for $D_R$ = 40%

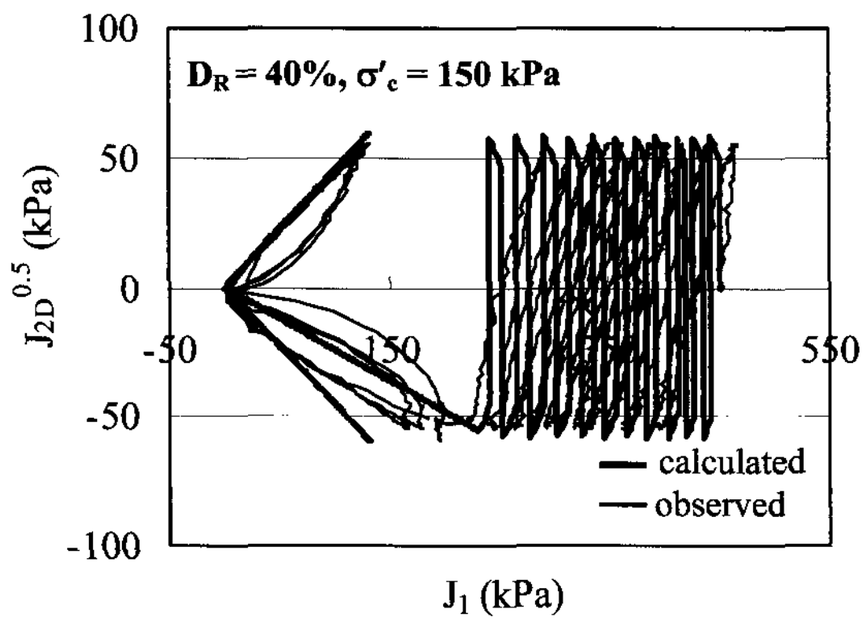


(e) effective stress paths for $D_R$ = 40%

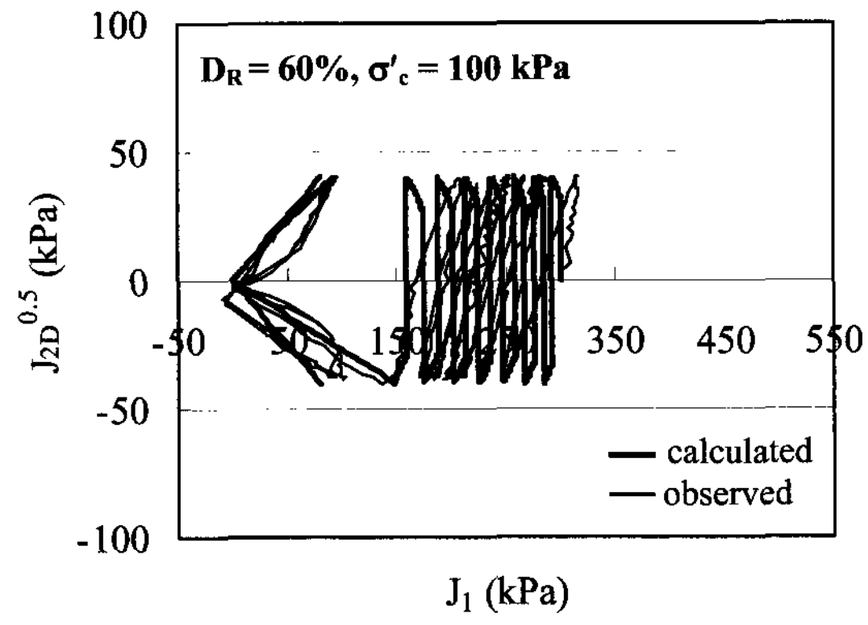


(f) effective stress paths for $D_R$ = 60%

Fig. 14. Calculated and observed cyclic soil responses with modified DSC model

liquefaction initiation point observed from experimental test results.

Fig. 14 shows calculated results using the modified DSC model. As shown in the figure, closer agreements are observed for excess pore pressure development and effective stress paths including the rapid stress degradation and initial liquefaction occurrence. Meanwhile, it is seen that observed stress-strain curves show bigger response in the strain than calculated stress-strain curves. This is because actual soils after initial liquefaction behave as a liquid material and thus produce large deformations with significant reductions of elastic modulus. Hence, further investigation and modification would be necessary if detailed deformation analyses were desired.

## 5. Conclusion

When a dynamic force such as an earthquake is applied to saturated sands, the excess pore pressure builds up continuously with decreases of soil strength, and sands are eventually liquefied. In this paper, the application of the DSC model to the analysis of liquefaction potential was examined through experimental and analytical investigations. While the DSC model has been successfully verified for many geotechnical dynamic problems, it has not been fully implemented for a whole process of liquefaction analysis, including definition of liquefaction potential.

For more realistic description of dynamic responses of saturated sands, the DSC model was modified based on two reference lines of the phase change and ultimate state lines that were observed from cyclic triaxial tests. Both static and cyclic undrained triaxial tests were performed for sands with different relative densities and confining stresses. Based on test results, a classification of liquefaction phases in terms of the dynamic effective stress path and the excess pore pressure development was proposed and adopted into the modified DSC model. The initial liquefaction and the critical disturbance $D_c$ in the modified DSC model is defined at a stage from which a rapid development of the excess pore pressure occurs with an effective stress path moving towards the zero-effective stress state along the phase change line. While values of the disturbance D in the original DSC model are obtained at every single cycle in the cyclic loading process, the procedure of the modified DSC model calculates values of D at every 1/4 cycle, including compression, unloading, extension, and unloading phases.

Compared with initial liquefaction, it is observed that the liquefaction resistance for a given soil from the original DSC model may be overestimated, which is unconservative. From the analysis results, it was seen that the predicted effective stress path, excess pore pressure, and stress strain curves using modified DSC model matches well measured results for the cyclic undrained triaxial tests. It was also found that the parameters required to define the model were simplified.

## Acknowledgements

This work has been supported by Yonsei University, Center for Future Infrastructure System, a Brain Korea 21 program, Korea.

## References

1. Desai, C.S. (1980), "A general basis for yield, failure and potential functions in plasticity", *International Journal of Numerical and Analytical Methods in Geomech*, 4, 361-375.
2. Desai, C.S. and Ma, Y. (1992), "Modeling of joints and interfaces using the disturbed state concept", *International Journal of Numerical and Analytical Methods in Geomech*, 16, 623-653.
3. Desai, C.S. and Toth, J. (1996), "Disturbed state constitutive modeling based on stress-strain and nondestructive behavior", *International Journal of Solids and Structure*, 33(11), 1619-1650.
4. Desai, C.S. and Rigby, D.B. (1997), "Cyclic interface and joint shear device including pore water pressure effects", *Journal of Geotechnical and Geoenvironmental Engineering*, 123(6), 568-579.
5. Desai, C.S., Sharma, K.G., Wathugala, G.W. and Rigby, D.B. (1991), "Implementation of hierarchical single surface $\delta_0$ and $\delta_1$ models in finite element procedure", *International Journal of Numerical and Analytical Methods in Geomech*, 15, 649-680.
6. Desai, C.S., Basaran, C. and Zhang, W. (1997), "Numerical algorithms and mesh dependence in the disturbed state concept", *International Journal of Numerical Method in Engineering*, 40, 3059-3083.
7. Desai, C.S., Park, I.J. and Shao, C. (1998), "Fundamental yet simplified model for liquefaction instability", *International Journal of Numerical and Analytical Methods in Geomech*, 22(7), 721-748.
8. Drucker, D.C. and Prager, W. (1952), "Soil mechanics and plastic analysis or limit design", *The Quarterly Journal of Mechanics and Applied Math*, 10(2), 157-165.
9. Finn, W.D.L., Lee, K.W. and Martin, G.R. (1977), "An effective

stress model for liquefaction", *Journal of Geotechnical Engineering Division*, ASCE, 103(6), 517-533.
10. Iai, S., Matsunaga, Y. and Kameoka, T. (1992), "Strain space plasticity model for cyclic mobility", *International Journal of Japan Society of Soil Mechanics and Foundation Engineering*, 32(2), 1-15.
11. Katti, D.R. and Desai, C.S. (1994), "Modeling and testing of cohesive soil using the disturbed state concept", *Journal of Engineering Mechanics*, ASCE, 121(1), 43-56.
12. Ladd, R.S. (1978), "Preparing test specimens using undercompaction", *Geotechnical Testing Journal*, GTJODJ, 1(1), 16-23.
13. Pal, S. and Wathugala, G.W. (1999), "Disturbed state model for sand-geosynthetic interfaces and application to pull-out tests", *International Journal of Numerical and Analytical Methods in Geomech*, 23(15), 1873-1892.
14. Roscoe, K.H., Scofield, A. and Wroth, C.P. (1958), "On yielding of soils", *Geotechnique*, 8, 22-53.
15. Seed, H.B., Idriss, I.M. and Arango, I. (1983), "Evaluation of liquefaction potential using field performance data", *Journal of Geotechnical Engineering Division*, ASCE, 109(3), 458-482.
16. Vade, Y.P. and Chern, J.C. (1983), "Effect of static shear on resistance of liquefaction", *Soil and Foundation*, 23(1), 47-60.
17. Youd, T.L., Idriss, I.M., Andrus, R.D., Arango, I., Castro, G., Christian, J.T., Dobry, R., Finn, W.D.L., Harder, L.F., Hynes, M.E., Ishihara, K., Koester, J.P., Liao, S.S.C., Marcuson III, W.F., Martin, G.R., Mitchell, J.K., Moriwaki, Y., Power, M.S., Robertson, P.K., Seed, R.B., Stokoe II, K.H. (2001), "Liquefaction resistance of soils: Summary report from the 1996 NCEER and 1998 NCEER/NSF workshops on evaluation of liquefaction resistance of Soils", *Journal of Geotechnical and Geoenvironmental Engineering*, ASCE, 127(10), 817-833.

(received on Oct. 19, 2007, accepted on Feb. 25, 2008)